# Investigation of the Gain Regimes and Gain Parameters of the Free Electron Laser Dispersion Equation

E. JERBY AND A. GOVER, SENIOR MEMBER, IEEE

*Abstract*—**We compute the small signal gain curve and various gain parameters by solving numerically the generalized gain-dispersion equation of free electron lasers (FEL), which characterizes the conventional magnetic bremsstrahlung FEL, as well as a large number of other FEL devices. The model includes high gain, collective, and axial velocity spread effects, and some waveguide effects. The FEL gain regimes are investigated and presented in terms of only three universal FEL characteristic parameters. The approximative analytic gain expressions are compared to the numerical computation results, and the approximation error is computed and displayed. In the intermediate regimes (high–low gain, tenuous–collective beam, cold–warm beam), the gain parameters are given in terms of useful curves, and a heuristic approximative formula is suggested for estimating the axial velocity spread gain reduction factor in all gain regimes. We also define and compute gain bandwidth and beam quality acceptance parameters in all gain regimes.**

## I. INTRODUCTION

FREE electron laser (FEL) schemes of various kinds have been demonstrated experimentally [1]–[7], and their small signal gain theory is well developed [8]–[20]. In all cases it can be shown that, to a good approximation, the same gain dispersion relation applies to all of them. This includes magnetic [10]–[13] and electrostatic [15], [16] bremsstrahlung FEL's, stimulated Compton scattering (electromagnetic pump) [8], transition radiation, Cerenkov and Smith–Purcell FEL's [17]–[21], and traveling wave amplifiers [22]. Furthermore, various plasma instabilities which involve interaction between space charge waves and electromagnetic waves are described by the same dispersion relation. This includes instabilities in a two-stream electron beam [23], [24] and in a rippled envelope electron beam [25], which were also considered as possible FEL mechanisms.

The basic model used to describe the FEL devices of various kinds consists of a transversely uniform *e*-beam and a waveguide structure with a uniform or axially periodic (in the case of Smith–Purcell FEL and TW amplifiers) cross section. The model also applies to free space electromagnetic modes which propagate along the *e*-beam axis without any waveguide structure, as long as the interaction length is short relative to a Rayleigh diffraction length, so that the electromagnetic beam cross section can be considered uniform. In all cases, the derivation of the small signal gain–dispersion relation is based on the assumption that the basic interaction involves a single electromagnetic mode which is phase matched or synchronized with excitations in the copropagating electron beam medium.

In some regimes (single electron interaction), the electrons in the beam interact individually with the electromagnetic modes. In other regimes (collective interaction regimes), the longitudinal space charge (plasma) waves participate in the interaction. What distinguishes the different FEL's from each other is only the means by which the electromagnetic wave is coupled and phase matched (synchronized) with the electron beam.

The basic FEL gain dispersion relation was investigated specifically for different kinds of FEL's by various authors (e.g., [10], [11], [18]–[22], [33]–[35]). It was investigated in a unified way for all FEL's in [9]. In various parameter domains, analytical approximations of the gain dispersion relation were found which led to explicit gain expressions for the FEL. These parameter domains, called gain regimes, are not only useful for computation of FEL gain and other parameters, but also correspond to different physical mechanisms in the FEL interaction process. Since the gain dispersion relation is similar for all FEL's, the gain regimes are also common.

In this paper, we identify distinctly the parameter domains of the different gain regimes. Using two computer programs, COLD and WARM (which were previously developed by Livni and Gover [25]), we solve numerically the gain–dispersion relation in the cold and warm beam limits and the intermediate regimes. We thus are able to check the validity of the analytical gain expressions and define accurately their validity domains. We present graphically the numerically calculated gain curves in the intermediate gain regimes.

The use of a small number of normalized operating parameters in our formulation (three constitutive parameters and a detuning parameter) enables us to discuss the transition between the different gain regimes and, particularly, the warm and cold gain-regimes in a unified way. This permits us, for example, to account for the main consequences of beam velocity spread and space charge effects in a general and simple way.

Finally, we present a number of curves for FEL parameters useful in FEL design. These parameters were calculated in the intermediate gain regimes by the same computer programs, and are useful for various FEL design applications.

Manuscript received November 30, 1984.

The authors are with the Faculty of Engineering, Tel-Aviv University, Ramat-Aviv, 69978, Israel.

0018-9197/85/0700-1041$01.00 © 1985 IEEE

## II. The FEL Gain-Dispersion Relation

Under the assumption of the model described in the previous section, we may describe the field of the electromagnetic mode which participates in the interaction as

$$\boldsymbol{E}(x, y, z) = a(o)\ \mathcal{E}(x, y)e^{ik_{zo}z}. \tag{1}$$

An exception is the Smith–Purcell FEL and TW amplifier, for which (1) describes only one of the components (space harmonics) which constitute the Floquet modes of a periodic waveguide.

When the electromagnetic mode interacts with the electron beam and they exchange power, the amplitude and phase of the electromagnetic mode vary along the interaction length ($z$-axis), and neglecting excitation of other electromagnetic modes, we assume

$$\boldsymbol{E}(x, y, z) = a(z)\ \mathcal{E}(x, y). \tag{2}$$

Substitution in the Maxwell equations produces the excitation equation for the mode amplitude $a(z)$:

$$\frac{d}{dz}\, a(z) - ik_{zo}\, a(z) = \frac{-1}{4\mathcal{P}} \int_{-\infty}^{\infty}\!\!\int J(x, y, z)\ \mathcal{E}^*(x, y)\, dx\, dy \tag{3}$$

where $\mathcal{P}$ is the total electromagnetic mode normalization power and $\boldsymbol{J}$ is the exciting alternate current in the electron beam.

To obtain the FEL gain-dispersion relation, one needs to solve, in addition to (3), the electron force equations (plasma equations) in order to find the ac current which is excited in the electron beam. This calculation differs for different FEL structures and different models for the plasma equations. However, in all cases when only the basic FEL interaction process is considered (neglecting additional effects due to diffraction, axial magnetic field, and other elaborations), does the same gain dispersion relation results in [9]

$$\bar{a}(s) = \frac{1 + \chi_p(\omega, s + ik_w)/\epsilon}{(s - ik_{z0})\,[1 + \chi_p(\omega, s + ik_w)]/\epsilon - i\kappa\chi_p(\omega, s + ik_w)/\epsilon} \cdot a(0) \tag{4}$$

where $\bar{a}(s)$ is the Laplace transform of the electromagnetic mode amplitude $a(z)$:

$$\bar{a}(s) = \int_0^{\infty} e^{-sz}\, a(z)\, dz. \tag{5}$$

$k_w = 2\pi/\lambda_w$ is the wavenumber of the periodic structure of period $\lambda_w$ which is employed in the FEL. In the case where no periodic waveguide or force is employed (as in the case in the Cerenkov FEL), we use $k_w = 0$.

The parameter $\kappa$ is the coupling coefficient which measures the strength of coupling between the electromagnetic wave and the electron beam. It is the only parameter in (4) which is characteristic of the different FEL's. It is tabulated in Table III for various kinds of FEL's. The various expressions for $\kappa$ are given or deduced from [9], [11], [15], [18]. The assumptions and the parameter definitions which are implied in these expressions are explained in Appendix A.

The longitudinal plasma susceptibility function $\chi_p(\omega, s)$ can be calculated from any appropriate model of plasma equations. We presently assume that the electron "gas" is described by the Vlasov equation, which is applicable in the general case of a warm electron beam. In such a model, the longitudinal plasma susceptibility is

$$\chi_p(\omega, s) = -i\frac{e^2}{\omega} \int_{-\infty}^{\infty}\!\!\int\!\!\int \cdot \frac{\partial g^{(0)}(P_x, P_y, P_z)/\partial P_z}{s - i\omega/v_z}\, dP_x\, dP_y\, dP_z \tag{6}$$

where $g^{(0)}(P_x, P_y, P_z)$ is the momentum distribution function of the electron beam. Integration over $P_x$, $P_y$ allows us to present $\chi_p$ in the normalized form:

$$\chi_p(\omega, s) = \frac{\epsilon}{2}\frac{k_D^2}{s^2}\, G'(\zeta) \tag{7}$$

where

$$G(\zeta) = \int_{-\infty}^{\infty} \frac{\bar{g}(x)}{x - \zeta}\, dx. \tag{8}$$

$\bar{g}(x)$ is the normalized longitudinal momentum distribution function defined by

$$\int_{-\infty}^{\infty}\!\!\int g^{(0)}(P_x, P_y, P_z)\, dP_x\, dP_y \equiv \frac{n_0}{P_{zth}}\, \bar{g}\left(\frac{P_z - P_{oz}}{P_{zth}}\right) \tag{9}$$

where

$$\zeta \equiv \frac{i\omega/s - v_{0z}}{v_{zth}}. \tag{10}$$

$k_D$ is the Debye wavenumber, defined by

$$k_D \equiv \sqrt{2}\,\frac{\omega_p'}{v_{zth}} \tag{11}$$

where $\omega_p'$ is the longitudinal plasma frequency,

$$\omega_p'^2 \equiv \frac{1}{\gamma_0\gamma_{0z}^2}\frac{e^2 n_0}{m\epsilon} \tag{12}$$

which was defined here in terms of the lab frame electron density $n_0 = I_0/(ev_{0z}A_e)$ ($I_0$ is the instantaneous beam current and $A_e$ is the $e$-beam cross-section area).

$$v_{zth} \equiv \frac{P_{zth}}{\gamma_0\gamma_{0z}^2 m} \tag{13}$$

$$\gamma_0 \equiv (1 - \beta_0^2)^{-1/2} \tag{14}$$

$$\gamma_{0z} \equiv (1 - \beta_{0z})^{-1/2}. \tag{15}$$

$v_{zth}$ and $P_{zth}$ are the longitudinal velocity and momentum spread of the electron beam. This spread can be the result of different causes, which are listed in Appendix B.

Often the electron distribution is approximated by a shifted Maxwellian distribution. In this case

$$\bar{g}(x) = \frac{1}{\sqrt{\pi}} e^{-x^2} \tag{16}$$

and

$$G(\zeta) = Z(\zeta) = \frac{1}{\sqrt{\pi}} \int_{-\infty}^{\infty} \frac{e^{-x^2}}{x - \zeta} dx \tag{17}$$

is the so-called plasma dispersion function which is tabulated in [28]. Maxwellian distribution (16) will be assumed in this paper whenever a warm beam (finite velocity spread) is considered.

In order to calculate the single path gain of the FEL, the inverse Laplace transform of (4) should be carried out:

$$a(z) = \frac{1}{2\pi i} \int_{\gamma - i\infty}^{\gamma + i\infty} \bar{a}(s)\, e^{sz}\, ds. \tag{18}$$

The electromagnetic power gain after length $z = L$ is then given by

$$\frac{P(L)}{P(0)} = \left|\frac{a(L)}{a(0)}\right|^2. \tag{19}$$

If the gain dispersion relation (4) has a finite number of poles $s_j$, then the inverse Laplace transform of (4) is given, in general, by

$$\frac{a(z)}{a(0)} = \sum_{j=1}^{N} A_j e^{s_j z} \tag{20}$$

where $A_j$ are the residues of (4) at the poles. In practice, the interaction of the electromagnetic wave with the electron beam is not strong enough to change the electromagnetic wave number substantially. We may thus write

$$s = ik_{z0} + i\delta k \tag{21}$$

where $|\delta k| << k_{z0}$. Substituting (21) in the expression for $\zeta$ (10), we can write

$$\zeta\,(s + ik_w) = \zeta_r + i\zeta_i \simeq \frac{\hat{\theta} - \delta k}{\theta_{th}} \tag{22}$$

where

$$\theta \equiv \omega/v_{z0} - k_{z0} - k_w \tag{23}$$

is the synchronism detuning parameter, and

$$\theta_{th} \equiv \frac{\omega}{v_{z0}} \cdot \frac{v_{zth}}{v_{z0}} \tag{24}$$

is the detuning spread parameter. This spread can be caused by a number of different reasons: the electron beam emittance, its energy spread and angular spread, and the transverse gradient of the wiggler magnetic field. The contributions of the various causes to the thermal spread parameter $\theta_{th}$ are derived and tabulated in Appendix B.

## III. The FEL Gain Regimes

The FEL gain calculation, based on the previous section formulation, is an elaborate process, involving an inverse Laplace transform computation. For many practical needs, one may derive analytic expressions for the gain using various approximations. We briefly describe the various gain regimes and derive the analytical gain expressions which are valid in each of them.

### A. Cold Beam Limit

A FEL electron beam is assumed to be cold for low enough detuning spread parameter values ($\theta_{th} \sim 0$) so that the condition $|\zeta| >> 1$ is satisfied. This condition, using (22), can be written as

$$[(\theta - \delta k_r)^2 + (\delta k_i)^2]^{1/2} >> \theta_{th}, \tag{25}$$

and the function $G(\zeta)$ (8) can be replaced by its asymptotic expansion:

$$\lim_{\zeta \to \infty} G(\zeta) = -1/\zeta. \tag{26}$$

We substitute definitions (10), (11), (23), and the definition of the space charge parameer, which is

$$\theta_p \equiv \frac{\omega_p'}{v_{0z}} \tag{27}$$

into (4) and get the "cold-beam" gain dispersion relation:

$$\bar{a}(s) = \frac{(s - ik_{z0} - i\theta)^2 + \theta_p^2}{(s - ik_{z0})\,[(s - ik_{z0} - i\theta)^2 + \theta_p^2] - i\kappa\,\theta_p^2} \cdot a(0). \tag{28}$$

This "transfer function" can be analytically inverted, since the poles are the nodes of the third-order dispersion equation

$$(s - ik_{z0})\,[(s - ik_{z0} - i\theta)^2 + \theta_p^2] - i\kappa\,\theta_p^2 = 0 \tag{29}$$

which can be explicitly solved and used in (19) and (20) to calculate the gain.

In order to find the roots of (28), it is often useful to substitute (21) into it. This results in a third-order algebraic equation with real coefficients:

$$\delta k\,(\delta k - \theta - \theta_p)\,(\delta k - \theta + \theta_p) + Q = 0 \tag{30}$$

where

$$Q \equiv \kappa\,\theta_p^2 \tag{31}$$

is the gain parameter.

This equation always has three real roots or one real root and two complex conjugate roots. In the second case, if the root with negative imaginary part satisfies $-\delta k_i >> 1$, the FEL operates in the high gain regime. The expo-

nential term which corresponds to this root in (20) dominates over the other two terms, which are neglected, and the gain is substantially exponential:

$$\ln \frac{P(L)}{P(0)} = 2 \ln |Aj| - 2\,\delta k_i L. \tag{32}$$

In the opposite limit or when all three roots are real, the gain cannot grow substantially, and this corresponds to the low gain regime for which

$$\frac{\Delta P}{P} = \frac{P(L) - P(0)}{P(0)} \ll 1. \tag{33}$$

For large enough values of the detuning parameter $\theta$, (33) is always satisfied. The FEL will be said to operate substantially at a low gain regime if (33) is satisfied for any $\theta$, and particularly in the maximum gain point $\theta = \theta_{max}$.

In order to develop the gain relations of the various gain regimes, it is useful to translate (28) from the $s$-plane into the $\delta k$ plane, as follows:

$$a(i\delta k) = \frac{(\delta k - \theta + \theta_p)(\delta k - \theta - \theta_p)}{i\delta k(\delta k - \theta + \theta_p)(\delta k - \theta - \theta_p) + iQ}. \tag{34}$$

It also proves useful to define at this point for later reference the FEL normalized operating parameters:

$$\bar{Q} = QL^3 \tag{35a}$$

$$\bar{\theta}_{th} = \theta_{th} L \tag{35b}$$

$$\bar{\theta}_p = \theta_p L \tag{35c}$$

$$\bar{\theta} = \theta L. \tag{35d}$$

In our present model, the FEL gain expression can be fully described by only these four parameters: the three normalized constitutive parameters $\bar{Q}$, $\bar{\theta}_{th}$, $\bar{\theta}_p$ and the normalized detuning parameters $\bar{\theta}$.

### B. High-Gain—Strong Coupling Regime

In the strong coupling high-gain regime, we assume that the complex wavenumber modification due to coupling ($\delta k$) is much greater than the wavenumber detuning parameter $|\theta|$, at which the FEL operates, so that the cold beam condition (25) is dominated by ($\delta k$). In addition, we also assume that $|\delta k|$ is much larger than the space charge parameter $\theta_p$: $|\delta k| \gg |\theta|, \theta_p, \theta_{th}$. Relation (34) may then be simplified into the form

$$\bar{a}(i\delta k) = \frac{(\delta k)^2}{i(\delta k)^3 + iQ} \cdot a(0) \tag{36}$$

or in a partial fraction form

$$\bar{a}(i\delta k) = \frac{a(0)}{3}\left[\frac{1}{i\delta k + iQ^{1/3}} + \frac{1}{i\delta k - \frac{i+\sqrt{3}}{2} Q^{1/3}} + \frac{1}{i\delta k - \frac{i-\sqrt{3}}{2} Q^{1/3}}\right]. \tag{37}$$

In the $s$-plane, the real part of the dominant pole of (37) is $(\sqrt{3}/2)\, Q^{1/3}$ and the amplitude gain becomes

$$\left|\frac{a(z)}{a(0)}\right| = \frac{1}{3} \exp\left(\frac{\sqrt{3}}{2} Q^{1/3} z\right). \tag{38}$$

The power gain in this case is

$$\frac{P(L)}{P(0)} = \frac{1}{9} \exp\left(\sqrt{3}\, \bar{Q}^{1/3}\right) \tag{39}$$

where the normalized gain parameter $\bar{Q}$ is defined in (35a). The original conditions $|\delta k| \gg \theta_p, \theta_{th}, |\theta|$ and $-\delta k_i L \gg 1$ may now be expressed in terms of the normalized FEL parameters:

$$\bar{Q}^{1/3} \gg \bar{\theta}_{th}, \bar{\theta}_p, |\bar{\theta}|, 1. \tag{40}$$

This is the condition for the parameters' domain of the "high-gain—strong coupling regime."

### C. High-Gain—Collective Regime

The FEL is said to operate in the high-gain collective regime when the space charge parameter $\bar{\theta}_p$ is much greater than the wavenumber modification $|\delta k|$:

$$\bar{\theta}_p \gg |\delta k|. \tag{41}$$

The maximum amplification, in this case, is expected to take place at the incidence of synchronism between the electromagnetic wave and the slow space charge wave ($\theta = -\theta_p$) [9]. We substitute these conditions ($\theta_p \gg |\delta k|$ and $\theta = -\theta_p$) into (34) and get

$$\bar{a}(i\delta k) = \frac{-i\delta k}{\delta k^2 + Q/(2\theta_p)} \cdot a(0). \tag{42}$$

In the $s$-plane, the dominant pole of (42) is $s_o = ik_{z0} + \sqrt{Q/2\theta_p}$ so the amplitude gain in the high gain limit is

$$\left|\frac{a(z)}{a(0)}\right| = \frac{1}{2} \exp\left(\sqrt{Q/2\theta_p} \cdot z\right). \tag{43}$$

The power gain is

$$\frac{P(L)}{P(0)} = \frac{1}{4} \exp\left(\sqrt{2\bar{Q}/\bar{\theta}_p}\right). \tag{44}$$

The combination of the original assumptions $-\delta k_i L \gg 1$ and $\theta_p \gg |\delta k|$ with the expression for the dominant pole $\delta k = -i\sqrt{Q/2\theta_p}$ and the cold beam condition $\delta k \gg \theta_{th}$ determines the parameters domain of the "high-gain space-charge dominated regime":

$$\bar{\theta}_p \gg \bar{Q}^{1/3} \gg 1 \tag{45a}$$

$$\bar{\theta}_p \gg \bar{\theta}_{th}. \tag{45b}$$

### D. Low-Gain Regimes

The derivation of the FEL low-gain regimes from the gain dispersion expressions (34) is described in detail in [9], [26]. The power output was expanded to the first order in $\bar{Q}$ for $\bar{Q} \ll \pi$, resulting in

$$\frac{P(L)}{P(0)} = 1 + \bar{Q} \cdot F(\bar{\theta}, \bar{\theta}_p). \tag{46}$$

The function $F(\bar{\theta}, \bar{\theta}_p)$ was found to be [26]

$$F(\bar{\theta}, \bar{\theta}_p) = \frac{1}{2\bar{\theta}_p}\left[\frac{\sin^2((\bar{\theta} + \bar{\theta}_p)/2)}{((\bar{\theta} + \bar{\theta}_p)/2)^2} - \frac{\sin^2((\bar{\theta} - \bar{\theta}_p)/2)}{((\bar{\theta} - \bar{\theta}_p)/2)^2}\right]. \tag{47}$$

In the "space charge dominated regime" where $\bar{\theta}_p >> \pi$, the function attains its maximum for any $\bar{\theta}_p$ at $\bar{\theta} = -\bar{\theta}_p$, and the maximum gain expression in this case is

$$G_{\max} = \frac{P(L)}{P(0)} = 1 + \bar{Q}/2\bar{\theta}_p. \tag{48}$$

For a tenuous beam, we neglect the space charge effect ($\theta_p \to 0$) and the function $F(\bar{\theta}, \bar{\theta}_p \to 0)$ reduces to

$$F(\bar{\theta}, \bar{\theta}_p \to 0) = \frac{d}{d\bar{\theta}}\left[\frac{\sin(\bar{\theta}/2)}{\bar{\theta}/2}\right]^2 \tag{49}$$

which attains its maximum at $\bar{\theta} = -2.6$. Thus, the maximum gain expression for the "tenuous beam—low-gain regime" becomes

$$G_{\max} = \frac{P(L)}{P(0)} = 1 + 0.27\,\bar{Q}. \tag{50}$$

### *E. The Warm Beam Limit*

The warm beam limit corresponds to the case when the longitudinal kinetic energy-spread of the electron beam is high enough so that inequality (25) is reversed. In the warm beam limit, we assume that the dominant pole of (4) is $s_0 = ik_{z0}$, which means that we neglect the change in the wavenumber caused by the space charge effects. Equation (4) can be written in the form

$$\bar{a}(s) = \left[(s - ik_{z0}) + \frac{i\kappa\,(\theta_p/\theta_{\text{th}})^2\,G'(\zeta)}{1 - (\bar{\theta}_p/\bar{\theta}_{\text{th}})^2\,G'(\zeta)}\right]^{-1} a(0). \tag{51}$$

When $\theta_{\text{th}} >> \theta_p$, which can also be written in the form $k_{z0} + k_w >> k_D$, where $k_D$ [see (11)] is the Debye wavenumber, we may approximate (51) by

$$\bar{a}(s) = [s - ik_{z0} - i\kappa\,(\theta_p/\theta_{\text{th}})^2\,G'(\zeta)]^{-1}\,a(0). \tag{52}$$

If we neglect the contribution of any poles which may be contributed by $G'(\zeta)$, then the inversion of (52) is straightforward, resulting in [17], [9]

$$\ln\frac{P(L)}{P(0)} = 2\,\frac{\bar{Q}}{\bar{\theta}_{\text{th}}^2}\,\text{Im}\;G'(\zeta) \tag{53}$$

where [using (8)]

$$\text{Im}\;G'(\zeta) = -\int_{-\infty}^{\infty} g'(x)\cdot\frac{\zeta_i}{(x - \zeta_r)^2 + \zeta_i^2}\,dx. \tag{54}$$

Since inequality (25) is reversed, it follows from (22) that $|\zeta_i| << 1$, and we may also substitute $s = ik_{z0}$ in the definition of $\zeta$ (10):

$$\zeta_r \simeq \zeta\,(ik_{z0} + ik_w) \simeq \left(\frac{\omega}{k_{z0} + k_w} - v_{0z}\right)/v_{z\text{th}} = \theta/\theta_{\text{th}}. \tag{55}$$

The integral in (54) then simplifies into $\text{Im}\;G'(\zeta) = \pi\,g'(\zeta_r)$, and the gain (53) is

$$G(\bar{\theta}) = \exp\left[2\,\frac{\bar{Q}}{\bar{\theta}_{\text{th}}^2}\,\pi\,g'\,(\bar{\theta}/\bar{\theta}_{\text{th}})\right]. \tag{56}$$

For a Gaussian electron momentum distribution (16), (54) attains its maximum when $\zeta_r = -1/\sqrt{2}$ so that $\text{Im}\;G'(-1/\sqrt{2}) \simeq 1.5$. The warm beam regime maximum gain expression is then given in terms of the normalized operating parameters (35) by

$$G_{\max} = \frac{P(L)}{P(0)} = \exp\,(3\bar{Q}/\bar{\theta}_{\text{th}}^2) \tag{57}$$

and in the low gain limit, by

$$G_{\max} = \frac{P(L)}{P(0)} = 1 + 3\bar{Q}/\bar{\theta}_{\text{th}}^2 \tag{58}$$

where we assume $\bar{Q} << \frac{1}{3}\,\bar{\theta}_{\text{th}}^2$.

When $\theta_p$ is of the same order of magnitude as $\theta_{\text{th}}$, we may not neglect it as before, and the dispersion equation in this case is the denominator of (51):

$$s - ik_{z0} + i\kappa\left(\frac{\theta_p}{\theta_{\text{th}}}\right)^2\frac{G'(\zeta)}{1 - \left(\frac{\theta_p}{\theta_{\text{th}}}\right)^2 G'(\zeta)} = 0. \tag{59}$$

If we assume again that (51) has only a single dominant pole and express it in terms of $\delta k$ (21), then for Gaussian distribution,

$$\delta k = -\frac{Q}{\theta_{\text{th}}^2}\,\frac{Z'(\zeta_r)}{1 - \left(\frac{\theta_p}{\theta_{\text{th}}}\right)^2 Z'(\zeta_r)}. \tag{60}$$

The power gain in this case is obtained from the general relation

$$\frac{P(L)}{P(0)} = \exp\,[-2\,\delta k_i L]. \tag{61}$$

The real and imaginary parts of the function $Z'(\zeta_r)$ are tabulated in [28] and plotted in [17] for a real argument $\zeta_r$. However, there is little advantage in calculating the gain in the "collective-warm" gain regime using the expressions (60) and (61), and in most cases for the intermediate cold-warm regimes, we will prefer to calculate the gain numerically or to use a general heuristic analytic approximation (71) (which is presented in the next chapter).

The formulas and the conditions of the maximum gain relations of the various gain regimes are summarized in Table I. One notices that when the detuning parameter $\bar{\theta}$ is chosen to maximize the gain, the gain expressions and the boundaries of the gain regimes can all be expressed in terms of merely three normalized operating parameters

TABLE I
THE GAIN DOMAINS AND MAXIMUM GAIN EXPRESSIONS

| | Gain regime | Parameter domain | Max. gain condition | Max. gain expression |
|---|---|---|---|---|
| I | Cold tenuous beam low-gain | $\bar{Q}, \bar{\theta}_p, \bar{\theta}_{th} < \pi$ | $\bar{\theta}_{max} = -2.6$ | $\frac{P(L)}{P(0)} = 1 + 0.27\,\bar{Q}$ |
| II | Space-charge-dominated low-gain | $\bar{\theta}_p > \frac{\bar{Q}}{2}, \bar{\theta}_{th}, \pi$ | $\bar{\theta}_{max} = -\bar{\theta}_p$ | $\frac{P(L)}{P(0)} = 1 + \bar{Q}/2\bar{\theta}_p$ |
| III | Collective-beam high-gain | $\frac{\bar{Q}/2 > \bar{\theta}_p > \bar{Q}^{1/3}, \bar{\theta}_{th}}{\bar{Q} > \pi}$ | $\bar{\theta}_{max} = -\bar{\theta}_p$ | $\frac{P(L)}{P(0)} = \frac{1}{4}\exp(\sqrt{2\bar{Q}/\bar{\theta}_p})$ |
| IV | Strong coupling high-gain | $\frac{\bar{Q}^{1/3} > \bar{\theta}_p, \bar{\theta}_{th}}{\bar{Q} > \pi}$ | $\bar{\theta}_{max} = -1.5$ | $\frac{P(L)}{P(0)} = \frac{1}{9}\exp(\sqrt{3}\,\bar{Q}^{1/3})$ |
| V | Warm beam | $\bar{\theta}_{th} > \bar{\theta}_p, \bar{Q}^{1/3}, \pi$ | $\bar{\theta}_{max} = -\frac{\bar{\theta}_{th}}{\sqrt{2}}$ | $\frac{P(L)}{P(0)} = \exp(3\bar{Q}/\bar{\theta}_{th}^2)$ |

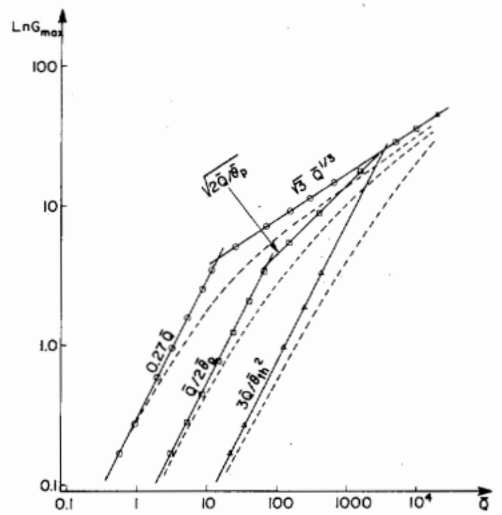


Fig. 1. The transition between the gain regimes as a function of $\bar{Q}$. The solid lines correspond to the analytic approximations for the maximum gain (Table I). The beam parameters are: ○—a cold beam ($\bar{\theta}_{th} = \bar{\theta}_p = 0$); □—a collective beam ($\bar{\theta}_{th} = 0$, $\bar{\theta}_p = 10$); △—a warm beam ($\bar{\theta}_{th} = 20$, $\bar{\theta}_p = 0$). The broken lines show for comparison the numerically computed curves for each case.

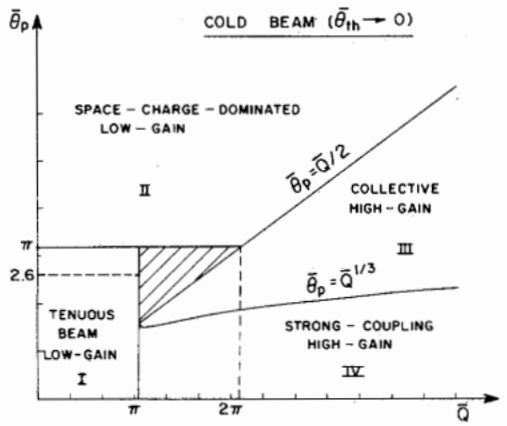


Fig. 2. The $\bar{Q} - \bar{\theta}_p$ plane map of the gain regimes for the case of a cold beam $\bar{\theta}_{th} \ll \pi$ (see Table I for the gain expressions).

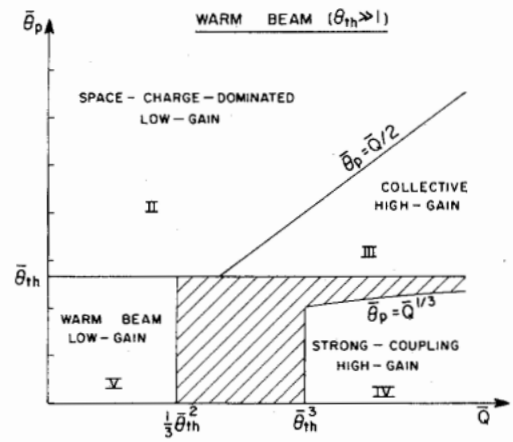


Fig. 3. The $\bar{Q} - \bar{\theta}_p$ plane map of gain regimes for a warm beam $\bar{\theta}_{th} \gg \pi$ (see Table I for the gain expressions).

$\bar{Q}, \bar{\theta}_p, \bar{\theta}_{th}$. Hence, the different gain regimes constitute different spatial regions in a three-dimensional space defined by these parameters. In order to illustrate the different boundaries of the gain regimes, we display in Fig. 1 the gain $G$ versus the gain parameters $\bar{Q}$ for three different choices of the FEL parameters $\bar{\theta}_p, \bar{\theta}_{th}$. The computer-calculated exact gain curves (broken lines) approach asymptotically to the approximate curves (solid lines) when the inequalities which define the various gain regimes are well satisfied.

An alternative figurative display of the different gain regimes is possible by drawing "cross-sectional cuts" in the $\bar{Q}, \bar{\theta}_p, \bar{\theta}_{th}$ parameter space. Fig. 2 maps the $\bar{Q} - \bar{\theta}_p$ plane for the case $\bar{\theta}_{th} = 0$. It describes the various cold beam gain regimes of $\bar{\theta}_{th} \ll \pi$. Fig. 3 displays another cut for an arbitrary $\bar{\theta}_{th} \gg \pi$. In this case, the "tenuous cold beam low-gain" regime is replaced by the "warm beam gain regime." The cold beam gain regimes, where $\bar{\theta}_p >$ $\bar{\theta}_{th}$ or $\bar{Q} > \bar{\theta}_{th}^3$, are similar to the corresponding regimes in the $\bar{\theta}_{th} = 0$ cut of Fig. 2, but extend over a smaller domain in the $\bar{Q} - \bar{\theta}_p$ plane.

## IV. The Transition Between Gain Regimes

The discussion on the various gain regimes and the analytic approximations for the gain in these regimes should

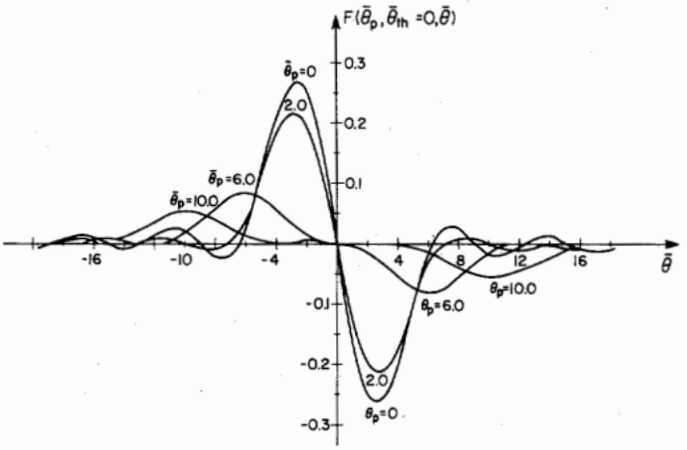


Fig. 4. The cold beam low-gain curves $F(\bar{\theta}, \bar{\theta}_{th} = 0, \bar{\theta})$ for various values of the normalized space charge parameter $\bar{\theta}_p$.

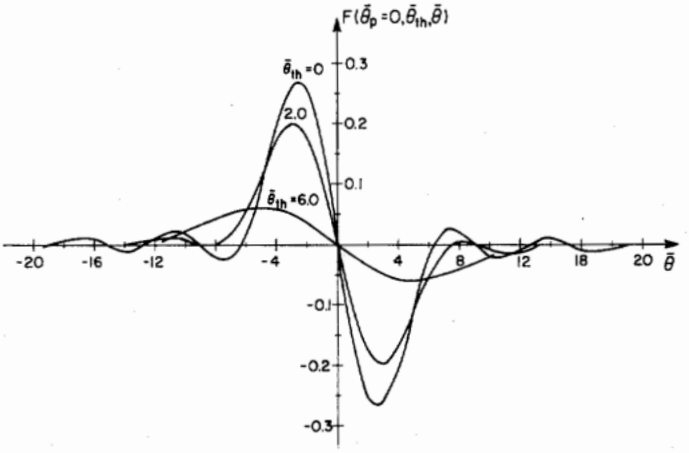


Fig. 5. The tenuous beam low-gain curves $F(\bar{\theta}_p = 0, \bar{\theta}_{th}, \bar{\theta})$ for various values of the normalized thermal spread parameter $\bar{\theta}_{th}$.

be followed by an evaluation of the accuracy of the given gain expressions. An error estimation has been done with the aid of graphic computer programs based on "COLD" and "WARM" subroutines [26]. The COLD subroutine calculates the inverse Laplace transform of the cold beam ($\theta_{th} = 0$) gain relation (28) by means of the residue method. It uses a standard formula for evaluating the roots of the third-degree algebraic equation (29) [27]. This is used to calculate the three residues $A_j$ of (28) and the amplitude gain $a(z)/a(0)$ (20). Fig. 4 shows, for example, the normalized low gain curves $F(\bar{\theta}, \bar{\theta}_{th} = 0, \bar{\theta}_p)$ (46) plotted by "COLD" for various values of $\bar{\theta}_p$.

The "WARM" subroutine has a more general validity but is slower. It has the ability to calculate the gain of a warm beam FEL for any value of the parameters $\bar{\theta}_{th}$, $\bar{\theta}_p$, $\bar{Q}$, $\bar{\theta}$. The subroutine performs an inverse Laplace transform of the gain-relation $\bar{a}(s)/a(0)$ [see (4)] by a direct numerical calculation of the Bromwich integral:

$$\frac{a(z)}{a(0)} = \frac{1}{2\pi i} \int_{\gamma - i\infty}^{\gamma + i\infty} \frac{\bar{a}(s)}{a(0)} e^{sz}\, ds. \tag{62}$$

The electron distribution is assumed to be Gaussian (i.e., $Z(x) = (1/\sqrt{\pi})\, e^{-x^2}$) so that $G(\zeta)$, which appeared in (7), is the well-known plasma dispersion function $Z(\zeta)$ (17), and can be written in the form [28]

$$Z(\zeta) = 2ie^{-\zeta^2} \int_{-\infty}^{i\zeta} e^{-z^2}\, dz, \qquad \text{Im}\,(\zeta) > 0. \tag{63}$$

The plasma dispersion function derivative $Z'(\zeta)$ is calculated by a subroutine, which was developed earlier by Burrel [29]. It approximates $Z'(\zeta)$ using two continued fraction formulas, one for small values of $\zeta$ and one for large values of $\zeta$. This technique greatly speeds up the subroutine, while keeping a relative error in the calculation to less than $6.0 \times 10^{-6}$. The numerical integration is performed by the method of Gaussian quadrature based on the orthogonal polynomials of Salzer [31]. The zeros of the polynomials and their corresponding weights are provided by Salzer [30] to 16 points, and by Stroud and Secrest to 24 points [32]. In all cases that we examined,

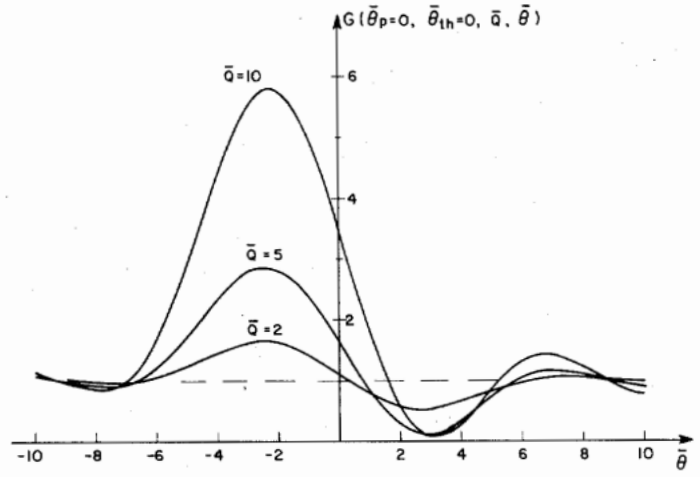


Fig. 6. The cold tenuous beam gain curves $G(\bar{\theta}_p = 0, \bar{\theta}_{th} = 0, \bar{Q}, \bar{\theta})$ for various values of the normalized gain parameter $\bar{Q}$.

there was good agreement between the results of program COLD and program WARM in their region of overlap $\theta_{th} \to 0$.

Fig. 5 shows the low gain curves $F(\bar{\theta}_p = 0, \bar{\theta}_{th}, \bar{\theta}) \equiv [G(\bar{\theta}_p, \bar{\theta}_{th}, \bar{\theta}) - 1]/\bar{Q}$, which were calculated using program WARM for $\bar{Q} \ll 1$ for various values of $\bar{\theta}_{th}$. Increasing $\bar{\theta}_{th}$ causes the $S$-shaped gain curve to be widened and lowered. The curve $\bar{\theta}_{th} = 0$ is identical to the one describing the analytical cold beam low-gain expression (49), and the curve $\bar{\theta}_{th} = 6$ already follows the analytic expression of the warm beam low-gain regime (56), (16).

As we increase the gain parameters $\bar{Q}$ beyond unity, we start approaching the high-gain regime. The $S$-shaped gain curve begins to lose its symmetry and we get amplification even for full synchronism ($\bar{\theta} = 0$), as shown in Fig. 6 for a few values of $\bar{Q}$ and $\bar{\theta}_{th} = \bar{\theta}_p = 0$. The $\bar{Q} = 2$ curve is similar to the low-gain curve (49) ($\bar{\theta}_{th} = 0$ in Fig. 5 and $\bar{\theta}_p = 0$ in Fig. 4).

Evidently, beam velocity spread leads to reduction in the FEL gain. Hence, the cold beam gain regimes $\bar{\theta}_{th} \simeq 0$ are of principal interest. The maximum gain (over all values of the detuning parameter $\bar{\theta}$) is determined in these regimes by only two parameters, $\bar{\theta}_p$ and $\bar{Q}$ [see (34)]. The

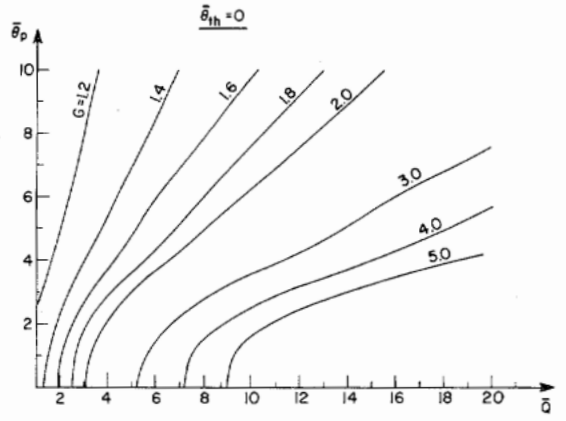


Fig. 7. Contour map of the cold beam FEL maximum gain $G_{max}$ in the $\bar{Q} - \bar{\theta}_p$ parameter plane.

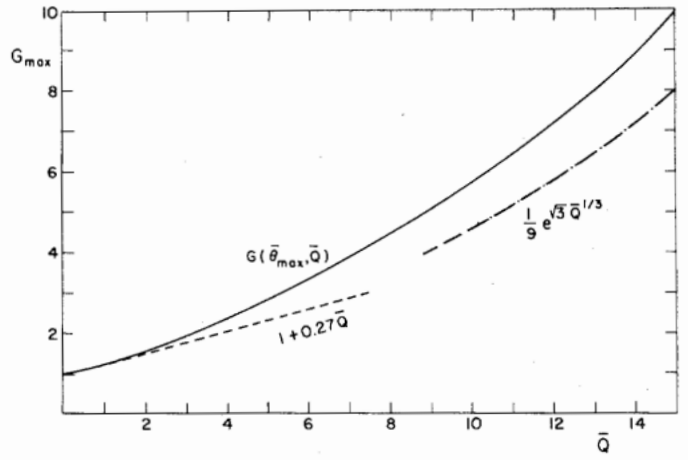


Fig. 8. The maximum gain $G_{max}$ versus $\bar{Q}$ for a cold tenous beam ($\bar{\theta}_p = \bar{\theta}_{th} = 0$). The broken line is the analytic approximation in the cold-beam, low-gain regime. The dashed-dotted line is the analytic approximation in the high-gain regime.

exact dependence of $G_{max}$ on the parameters $\theta_p$, $Q$ was calculated using subroutine COLD, and is displayed in Fig. 7 in terms of constant gain contours in the $\bar{Q} - \bar{\theta}_p$ plane. The right-bending of the equigain curves in the map indicates the existence of space charge gain depression in both low- and high-gain regimes. Note, however, that the parameter $\bar{Q}$ is not independent of $\bar{\theta}_p$ ($\bar{Q} = \kappa\bar{\theta}_p^2 L$). Hence, the monotonous reduction in gain, as $\bar{\theta}_p$ grows and $\bar{Q}$ stays constant, happens only if the interaction parameter $\kappa L$ is decreased in inverse ratio to $\bar{\theta}_p^2$ in order to keep $\bar{Q}$ constant. When $\kappa L$ is kept constant, the gain always increases with $\bar{\theta}_p$.

In many practical cases, the beam current density, the velocity spread, and the interaction length are small enough to permit the assumptions $\bar{\theta}_p = 0$, $\bar{\theta}_{th} = 0$. The maximum gain $G_{max}$ is then a function of only one single parameter $\bar{Q}$. This dependence is plotted in Fig. 8 as a function of the gain parameter $\bar{Q}$ in the regime $0 < \bar{Q} < 15$. The analytic expression for the maximum gain in the low gain regime [see (50)] is illustrated for comparison in Fig. 8 by a broken line. It fits the exact gain curve along its tangent at the origin in the regime $\bar{Q} < 2$. For high

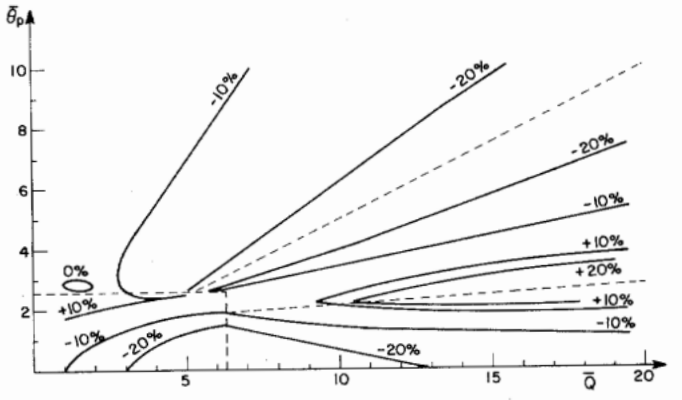


Fig. 9. A contour map of the relative approximation error [see (64)] of the analytic gain expressions with respect to the exact calculation of a cold beam FEL gain in the various gain regimes. The broken lines are the borders between the gain regimes (compare Fig. 2).

$\bar{Q}$ values, the FEL starts getting into the high-gain regime where the gain is exponential, but for $\bar{Q} < 15$ it still deviates by more than 20 percent from the high-gain regime analytic expression (39), which is shown in Fig. 8 by the dashed-dotted line.

We note that this deviation does not converge to zero even for higher values of $\bar{Q}$. The reason for this failure of the analytic expression can probably be traced to the assumption $\bar{\theta} \simeq 0$, which was made during its derivation [in (36)]. As we show later in Fig. 15, the numerical calculation indicates that the maximum gain point in the high-gain regime tends to a value $\bar{\theta}_{max} \simeq -1.5$, and for a large range of $\bar{Q}$ values, we find that the gain at this point is larger than its value at $\bar{\theta} = 0$ by at least 5 percent.

Using the exact gain calculation with programs COLD and WARM, we have evaluated the error involved in using the analytic gain expressions (Table I) corresponding to all gain regimes. The equi-error contours in all cold gain regimes occurring for beam spread parameter value $\bar{\theta}_{th} = 0$ are plotted in Fig. 9 in the $\bar{Q} - \bar{\theta}_p$ plane. The relative error in the maximum incremental gain is defined by

$$ER(\bar{Q}, \bar{\theta}_p) = \frac{G^*_{max}(\bar{Q}, \bar{\theta}_p) - G_{max}(\bar{Q}, \bar{\theta}_p)}{G_{max}(\bar{Q}, \bar{\theta}_p) - 1} \qquad (64)$$

where $G_{max}(\bar{Q}, \bar{\theta}_p)$ is the exact numerically computed value of the maximum gain at the point $(\bar{Q}, \bar{\theta}_p)$ and $G^*_{max}$ is the approximate value of the gain at this same point. resulting from the analytic expression.

Inspection of Fig. 9 shows that when the parameter conditions listed in Table I are satisfied, the error involved with the approximate gain calculation is less than $\pm 20$ percent for all the cold beam FEL gain regimes. The approximation error in the transition region between any two gain regimes (excluding the transition between the low-gain tenuous beam regime and the space charge dominated gain regimes) is greater than 20 percent (typically 30–40 percent).

The borders between the gain regimes in Fig. 9 are roughly the same as in Fig. 2. However, in order to minimize the errors in using the analytical expressions, we

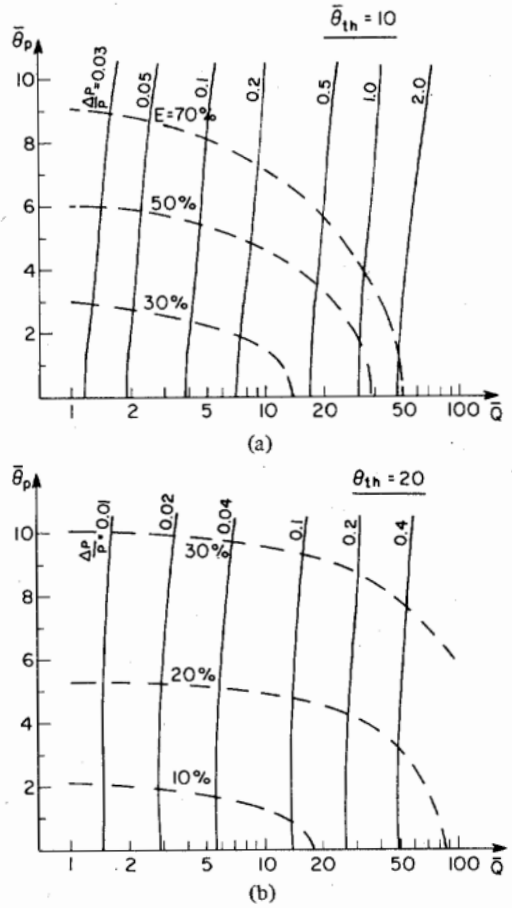


Fig. 10. Maximum gain contour maps in the $\bar{Q} - \bar{\theta}_p$ parameter plane in the warm-beam regimes. (a) $\bar{\theta}_{th} = 10$. (b) $\bar{\theta}_{th} = 20$. The broken lines show the relative error of the analytic expression (57) with respect to the exact calculation.

slightly modified the borders of the tenuous beam low-gain regime to be $\bar{Q} = 2\pi$, $\bar{\theta}_p = 2.6$.

At values of the thermal spread parameter $\bar{\theta}_{th} >> \pi$, the FEL may operate at cold or warm gain regimes, depending on the values of the other operating parameters $\bar{\theta}_p$, $\bar{Q}$. In Fig. 10(a) and (b), we show the numerically calculated gain contour maps for $\bar{\theta}_{th} = 10$ and $\bar{\theta}_{th} = 20$, respectively. The broken lines indicate the relative error contours, calculated by (64). It is seen that in the "warm beam—low-gain" regime ($\bar{\theta}_{th} >> \bar{\theta}_p$, $\bar{Q} << \bar{\theta}_{th}^2$), the relative error is moderate ($\sim$20 percent), but in the intermediate regimes it becomes substantially greater. This may limit the usefulness of the warm beam analytic expression ($G = \exp(3\bar{Q}/\bar{\theta}_{th}^2)$) to the "low-gain–warm beam" regime only.

In many practical situations, especially when considering RF linacs with tenuous beams, the limit $\bar{\theta}_p << 1$ is applicable. For this reason, we draw in Fig. 11 the contour map of the maximum gain numerically calculated in the parameter space plane $\bar{Q} - \bar{\theta}_{th}$, $\bar{\theta}_p = 0$. This map is useful to estimate the reduction in gain due to axial velocity spread, which takes place when the electron beam quality is not high enough, and when one tries to operate an FEL at shorter and shorter wavelengths (VUV, X-ray FEL's) [41]. The parameter domain of the map ($\bar{\theta}_{th} < 10$, $\bar{Q} <$ 100) covers the intermediate cold–warm tenuous beam regime at which $\bar{\theta}_{th}$ is not high enough to make the warm beam gain formula $G = \exp(3\bar{Q}/\bar{\theta}_{th}^2)$ (row 5 of Table I) applicable. We found that even for $\bar{\theta}_{th} = 10$, the analytic formula deviates by more than 25 percent from the exact gain given by the numerically computed contours, and therefore, the contours should be used to calculate the gain reliably in this regime.

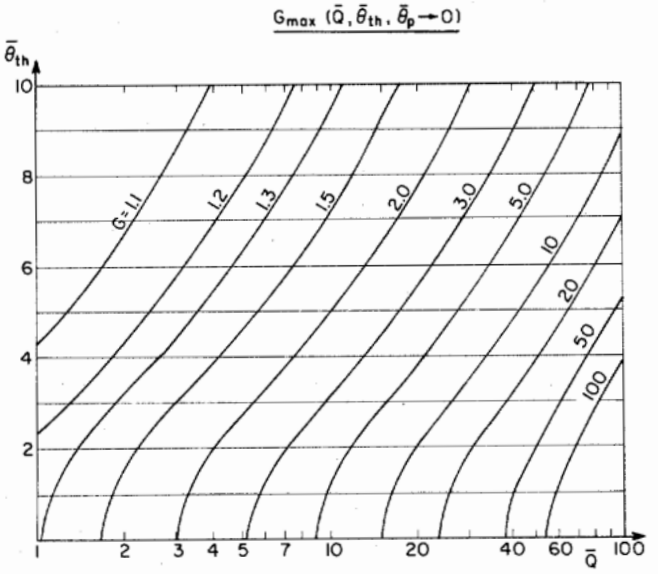


Fig. 11. Maximum gain contour map in the $\bar{Q} - \bar{\theta}_{th}$ parameter plane for a tenuous beam ($\theta_p \to 0$) FEL. These contours also describe the detuning spread acceptance parameter $\bar{\theta}_{th}^{ac}$ according to definition (67).

### A. Acceptance Criteria for $\bar{\theta}_{th}$

The gain reduction due to axial velocity spread is, of course, an undesirable effect. Often it cannot be avoided because of the insufficient quality of the electron beam, which results because of various reasons (Appendix B). It is useful to define acceptance criteria for $\bar{\theta}_{th}$ which will give an estimate of how small the parameter $\bar{\theta}_{th}$ should be kept so that the actual gain will not be substantially lower than the cold beam gain. The maximum value of $\bar{\theta}_{th}$ to satisfy this requirement would be termed the "detuning spread acceptance parameter," $-\bar{\theta}_{th}^{ac}$ [41].

Three different definitions for $\bar{\theta}_{th}^{ac}$ are useful for various applications. According to the first definition, the incremental gain at $\bar{\theta}_{th} = \bar{\theta}_{th}^{ac}$ falls to half its value in a cold beam ($\bar{\theta}_{th} = 0$):

$$\frac{G(\bar{\theta}_{th}^{ac}) - 1}{G_{cold} - 1} = \frac{1}{2}. \tag{65}$$

In the second definition, the logarithmic gain at $\bar{\theta}_{th} = \bar{\theta}_{th}^{ac}$ falls to half its value in a cold beam:

$$\frac{\ln G(\bar{\theta}_{th}^{ac})}{\ln G_{cold}} = \frac{1}{2}. \tag{66}$$

The detuning parameter acceptance $\bar{\theta}_{th}^{ac}$ according to both definitions is shown in Fig. 12. The curves are drawn on log–log scale for a large range of values in the limit $\theta_p \to 0$. Note that for $\bar{Q} << \pi$, $\ln G \simeq G - 1$ and both definitions coincide, as is also seen in the drawing.

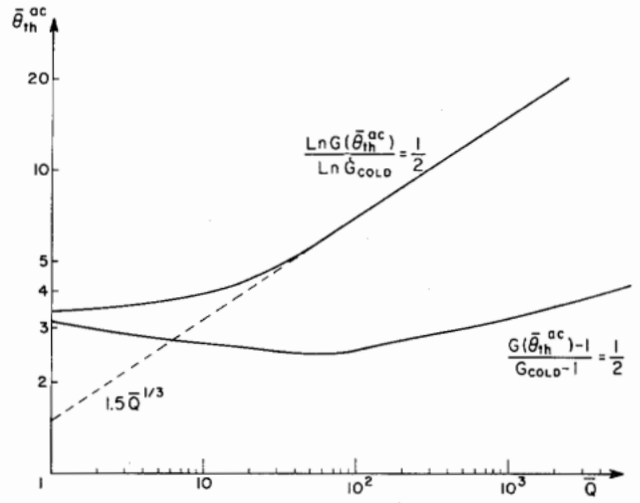


Fig. 12. The detuning spread acceptance parameter $\bar{\theta}_{th}^{ac}$ for two different definitions, (65) and (66) in the limit $\bar{\theta}_p \to 0$. Only the second definition tends to the asymptotic limit [see (70)].

A third possible definition for $\bar{\theta}_{th}^{ac}$ requires reduction of the FEL gain from its cold beam value to a set constant gain value:

$$G(\bar{\theta}_{th}^{ac}) = \text{const.} \tag{67}$$

Such a definition is especially useful in FEL oscillator designs, where the constant in (67) would be $1/R$ where $R$ is the round-trip power reflection coefficient of the cavity. $\bar{\theta}_{th}^{ac}$ according to this definition is the highest detuning spread for which oscillation (lasing) is still possible. Fig. 11 shows curves of $\bar{\theta}_{th}^{ac}$ according to the last definition for various constants in the limit $\bar{\theta}_p \to 0$.

It is natural to assume that the borders between the warm beam gain regimes and the cold beam gain regimes should define the acceptance criteria [10]. From Table I we get the borders between the cold and warm low-gain regimes:

$$\bar{\theta}_{th}^{ac} = \pi \tag{68}$$

and for the high-gain regimes:

$$\bar{\theta}_{th}^{ac} = \bar{Q}^{1/3}. \tag{69}$$

These common approximations for the acceptance parameter can now be checked against the numerically computed curves for $\bar{\theta}_{th}^{ac}$ according to the different definitions (Fig. 12). Clearly, in the limit $\bar{Q} \ll \pi$, both definitions (65), (66) shown in Fig. 12 are identical and tend to the asymptotic value $\bar{\theta}_{th}^{ac} \simeq \pi$ in accordance with (68). It is evident that the high-gain regime approximate expression for the detuning spread acceptance $\bar{\theta}_{th}^{ac} = \bar{Q}^{1/3}$ (69) does not correspond at all to the common definition of acceptance given by (65). However, for $\bar{Q} > 30$, it seems that the top curve (66) is at least proportional to $\bar{Q}^{1/3}$, indicating that in this regime, the predominant effect of the thermal spread is to reduce the exponential factor $\delta k_i L$. The best asymptotic fit to the numerically calculated curve is

$$\bar{\theta}_{th}^{ac} = 1.5\,\bar{Q}^{1/3} \tag{70}$$

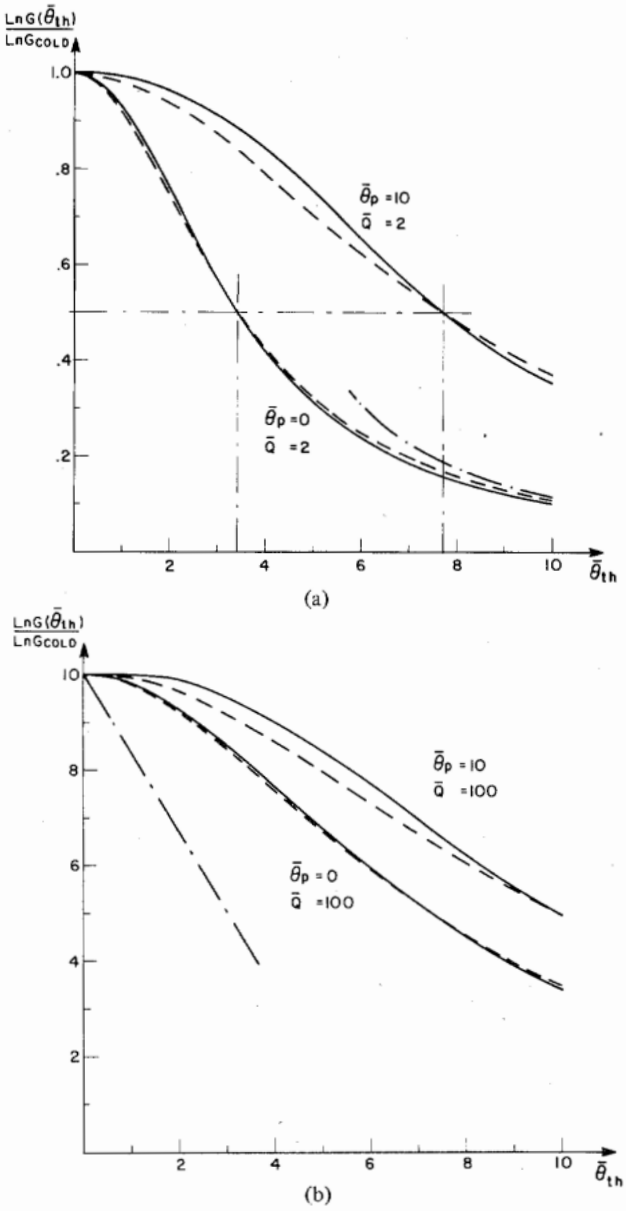


Fig. 13. The gain reduction factor due to axial velocity spread for (a) low-gain examples ($\bar{Q} = 2$) and (b) high-gain examples ($\bar{Q} = 100$). In each case we show a tenuous beam ($\bar{\theta}_p = 0$) and a space charge dominated beam ($\bar{\theta}_p = 10$) example. The solid lines display the results of the numerical computation. The broken lines display the heuristic formula (71). The dashed dotted line in (a) shows for comparison the warm beam limit gain reduction factor $11.1/\bar{\theta}_{th}^2$ derived from (50) and (57). The dashed dotted line in (b) shows for comparison the prediction of [39] [see (72)].

which can be used instead of (66) for estimating the exponential gain detuning spread acceptance in the regime $\bar{Q} > 30$.

### *B. The Transition Between the Cold and the Warm Gain Regimes*

As was previously shown, the analytic gain expressions are limited in their aptitude for estimating the gain in the intermediate region between the cold and warm gain regimes, and the gain in these regions should be calculated numerically using program WARM. Fig. 13(a) and (b) shows the numerically computed reduction factor of the maxi-

TABLE II
THE WORKING FORMULAS FOR ESTIMATING THE FEL GAIN IN THE INTERMEDIATE COLD-WARM TENUOUS BEAM GAIN REGIMES

| | Intermediate regime | Parameter conditions | $\bar{\theta}_{th}^{ac}$ | Max. gain expression |
|---|---|---|---|---|
| I | Cold-warm tenuous beam low-gain | $\bar{Q}, \bar{\theta}_p < \pi$ | $\pi$ | $\frac{P(L)}{P(0)} = 1 + \frac{0.27\,\bar{Q}}{1 + \bar{\theta}_{th}^2/\pi^2}$ |
| II | Cold-warm strong coupling | $\bar{Q} > \bar{\theta}_p^3, \pi$ | $1.5\,\bar{Q}^{1/3}$ | $\frac{P(L)}{P(0)} = \exp\left(\frac{\sqrt{3}\,\bar{Q}^{1/3} - \ln 9}{1 + \bar{\theta}_{th}^2/2.25\,\bar{Q}^{2/3}}\right)$ |

mum FEL gain as a function of the axial velocity spread for various values of $\bar{Q}$ and $\bar{\theta}_p$. These curves indicate that the gain reduction factor variation as a function of $\bar{\theta}_{th}$ depends on the parameters $\bar{\theta}_p$. This conclusion is in agreement with [42] and in disagreement with [39]. We also note that all the curves must converge in the asymptotic limit $\bar{\theta}_{th} >> \pi$ to the warm beam gain expression $\ln G(\bar{\theta}_{th}) = 3\bar{Q}/\bar{\theta}_{th}^2$ (57).

We propose here a practical heuristic formula for the estimate of the gain in the intermediate warm gain regime:

$$\frac{\ln G(\bar{\theta}_{th})}{\ln G_{cold}} = \frac{1}{1 + (\bar{\theta}_{th}/\bar{\theta}_{th}^{ac})^2} \tag{71}$$

where $\bar{\theta}_{th}^{ac}$ is defined for each case by (66). The curves corresponding to this expression are drawn in a broken line in Fig. 13(a) and (b), and are compared to the numerically calculated gain curves. By definition, the curve of (71) is identical with the numerically computed curve around the points $\bar{\theta}_{th} = 0$ and $\bar{\theta}_{th} = \bar{\theta}_{th}^{ac}$. Equation (71) also converges close to the warm beam expression $\ln G(\bar{\theta}_{th}) = 3\bar{Q}/\bar{\theta}_{th}^2$ [dashed-dotted curve in Fig. 13(a)] in the asymptotic limit $\bar{\theta}_{th} >> \bar{\theta}_{th}^{ac}$. This can be shown, for example, in the low-gain regime using (50) and (68) for $\ln G_{cold}$ and $\bar{\theta}_{th}^{ac}$, respectively, and in the high-gain regime using (39) and (70) (see Table II).

Inspection of Fig. 13(a) and (b) indicates that the curve based on (71) indeed fits the numerically computed curve for $\bar{\theta}_p \to 0$ very well, and it deviates from the numerically computed curve by less than 5 percent at larger values of the parameter $\bar{\theta}_p$ that we checked ($\bar{\theta}_p < 10$). This makes (71) a useful formula to predict the gain reduction due to axial velocity spread without numerical computation. For arbitrary FEL parameters, one only needs to calculate the value of $G_{cold}(\bar{Q}, \bar{\theta}_p)$, which can be accomplished using Table I or Fig. 7, and then find the value of $\bar{\theta}_{th}^{ac}(\bar{Q}, \bar{\theta}_p)$ of (66) using the numerically computed curves of Fig. 14. These parameters result straightforwardly in the general gain $G_{max}(\bar{Q}, \bar{\theta}_p, \bar{\theta}_{th})$ when plugged in (71). It should be noted, though, that since $\bar{\theta}_{th}^{ac}$ of Fig. 14 was computed specifically for a shifted Maxwellian electron velocity distribution, this procedure for calculating the gain in the intermediate warm regime is valid only when the actual *e*-beam velocity spread can be represented by such a distribution function.

An alternative approximate formula for the axial velocity spread gain reduction factor was proposed in [39] for a Lorentzian velocity distribution function. Written in terms of the present paper terminology, this formula reads:

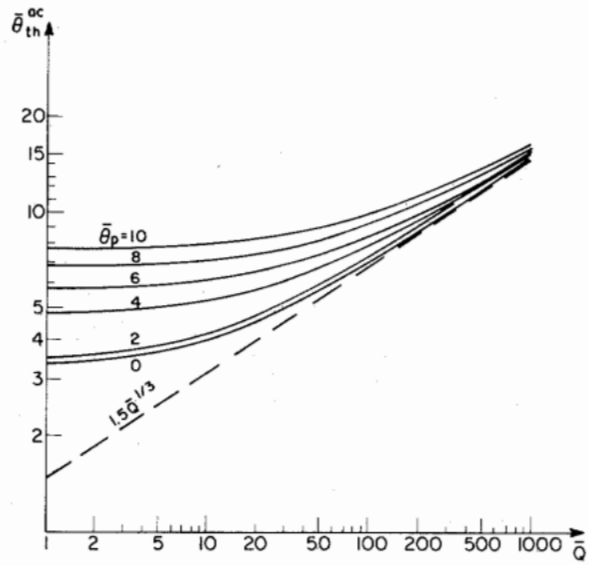


Fig. 14. The detuning acceptance parameter $\bar{\theta}_{th}^{ac}$ according to the definition of (66) for various values of $\bar{\theta}_p$. For $\bar{Q} >> \pi$, all curves approach asymptotically to the analytical expression (70) (in broken line).

$$\frac{G(\bar{\theta}_{th}) - 1}{G_{cold} - 1} = e^{-\bar{\theta}_{th}}. \tag{72}$$

This reduction factor is also displayed in Fig. 13(b), in dashed-dotted lines, for the purpose of comparison with our numerically computed curves. We see that (72) predicts a much stronger reduction in gain than predicted by our numerically computed curves. (Perhaps the reason is the high content of electrons in the distribution tails when a Lorentzian distribution is assumed.) Also, the reduction rate of (72) is independent of $\bar{\theta}_p$, in contrast to our numerically computed curves.

Working formulas for estimating the cold-warm intermediate regime gain, according to our heuristic approximation (71), are given explicitly in Table II, which is valid specifically for a tenuous beam and occurrence of low (I) or high (II) gain conditions.

## V. THE GAIN DETUNING AND BANDWIDTH PARAMETERS

The formulation used in the present particle fully describes the FEL gain as a function of the detuning param-

eter $\bar{\theta} = [\omega/v_{z0} - k_{z0}(\omega) - k_w]L$ (23), (35d) for any given FEL parameters $\bar{Q}$, $\bar{\theta}_p$, $\bar{\theta}_{th}$. The gain function [Fig. 17(a)] attains a maximum value $G_{max}$ at $\bar{\theta} = \bar{\theta}_{max} < 0$ near the synchronism point $\bar{\theta} = 0$. The gain function, drawn as a function of the detuning parameter $\bar{\theta}$, usually has a narrow width. Consequently, the dependence of the gain on both the frequency and the velocity (energy) is determined predominantly by its dependence on $\bar{\theta} = \bar{\theta}(\omega, v_z)$. Although the other parameters may also depend on frequency and velocity, their values vary only slightly for frequencies or velocities corresponding to the detuning parameter bandwidth $\Delta\bar{\theta}$.

The explicit dependence of $\bar{\theta}$ on $\omega$ is found when $k_z(\omega)$ is substituted in (23). In a waveguide structure

$$k_z(\omega) = (\omega^2 - \omega_{c0}^2)^{1/2}/c \tag{73}$$

whereas in free space $k_z = \omega/c$. In the latter case, the dependence of $\bar{\theta}$ on $\omega$ is linear and the gain curve dependence on $\bar{\theta}$ is similar to its dependence on $\omega$. This is also the case in a waveguide, when the two solutions to the equation $\bar{\theta}(\omega) = 0$ are well spaced. (The opposite limit is discussed later in Section V-B.) The dependence of $\bar{\theta}$ on velocity (energy) is given in terms of $v_z = [v^2 - (e\bar{A}_w/\gamma mc)^2]^{1/2}$ where $\gamma = E/mc^2 = (1 - \beta^2)^{-1/2}$. This dependence can also be considered linear within the narrow velocity (energy) range corresponding to $\Delta\bar{\theta}$. Thus, the gain curve as a function of $\bar{\theta}$ closely resembles its dependence on $v(\gamma)$.

### A. Detuning Bandwidth Parameters

Assuming the linear approximations are valid, the computation of the detuning parameter bandwidth $\Delta\bar{\theta}$ can be used to calculate two useful parameters [9]. The bandwidth gain frequency bandwidth is

$$\Delta\omega = (v_{z0}^{-1} - v_{g0}^{-1})^{-1} \frac{\Delta\bar{\theta}}{L} \tag{74}$$

where

$$v_{g0} = \left.\frac{d\omega}{dk_z}\right|_{\omega_0} = c\left(1 - \frac{\omega_{c0}^2}{\omega_0^2}\right)^{1/2}$$

is the group velocity of the electromagnetic wave in the waveguide. In the limit of free space propagation, $v_{g0} = c$ and (74) reduces to the simple relation

$$\frac{\Delta\omega}{\omega} = \frac{1}{2N_w}\frac{\Delta\bar{\theta}}{\pi} \tag{75}$$

where $N_w = L/\lambda_w$ is the number of wiggles in the wiggler. The second useful parameter that can be calculated from the parameter $\Delta\bar{\theta}$ is the energy (or velocity) detuning bandwidth:

$$\frac{\Delta\gamma}{\gamma_0} = \beta_{z0}^2\gamma_{z0}^2\frac{\Delta v_z}{v_{z0}} = \beta_{z0}^2\gamma_{z0}^2\frac{\lambda}{2L}\frac{\Delta\bar{\theta}}{\pi}. \tag{76}$$

In the limit of free space propagation, $\lambda = \lambda_w(\beta_{z0}^{-1} - 1)$ and

$$\frac{\Delta\gamma}{\gamma_0} = \frac{\beta_{z0}}{1 + \beta_{z0}}\frac{1}{2N_w}\frac{\Delta\bar{\theta}}{\pi} \simeq \frac{1}{4N_w}\frac{\Delta\bar{\theta}}{\pi}. \tag{77}$$

The second part of the last equality applies in the highly relativistic limit $\gamma_{z0} >> 1$.

The frequency bandwidth parameter (75) is useful for estimating the FEL amplifier bandwidth. In an oscillator, it helps to calculate the effective spontaneous emission power useful to build up the oscillation [40].

The energy detuning bandwidth parameter is useful as an electron beam energy stability acceptance parameter (to be distinguished from the energy spread acceptance parameter). This parameter indicates to what extent the beam energy may deviate from the energy corresponding to $\bar{\theta}_{max}$ and still povide appreciable gain at frequency $\omega$ (the beam itself may be nonenergetic). Such an energy stability acceptance parameter may be useful, for instance, for RF linac FEL oscillator design. Due to amplitude and phase instability of the klystrons, which drive the accelerator cavities, the different microbunches of which the accelerated beam macropulse consists may be accelerated to different velocities. In extreme cases, some microbunches may attenuate radiation which was generated by previous microbunches and was stored in the cavity. To assure continuous buildup of the power in the cavity, the variance in microbunches energy should be limited by (77).

As in the definition of $\bar{\theta}_{th}^{ac}$, we offer here two alternative definitions to $\Delta\bar{\theta}$. One corresponds to the detuning width at half the maximum incremental gain point:

$$G_{ac}(\bar{\theta}_{1,2}) - 1 = \tfrac{1}{2}(G_{max} - 1). \tag{78}$$

The other definition relates to the logarithmic gain:

$$\ln G_{ac}(\bar{\theta}_{1,2}) = \tfrac{1}{2}\ln G_{max} \tag{79}$$

where

$$\Delta\bar{\theta} = |\bar{\theta}_2 - \bar{\theta}_1|. \tag{80}$$

Both definitions coincide in the low gain regime $G_{max} - 1 << 1$. The definitions of $\bar{\theta}_1$, $\bar{\theta}_2$, and $\Delta\theta$ are depicted in Fig. 17(a).

Assuming $\bar{\theta}_p \to 0$, the parameter $\Delta\bar{\theta}$ is dependent only on the parameters $\bar{Q}$ and $\bar{\theta}_{th}$. For the practical limit of a cold beam $\bar{\theta}_{th} \to 0$, the dependence of $\Delta\bar{\theta}$ on the parameter $\bar{Q}$ was computed and displayed in Fig. 15 for both definitions (78) and (79). In the low gain limit, both curves converge to the limit $\Delta\bar{\theta} \simeq \pi$ ($\simeq \bar{\theta}_{th}^{ac}$), and (75) and (77) reduce to the conventional expressions for the frequency and energy detuning bandwidths [9]–[11] $\Delta\omega/\omega = \Delta E/E = (2N_w)^{-1}$. In the high gain regime ($\bar{Q} >> \pi$), both curves behave in irregular ways, which are substantially different from the corresponding detuning spread parameter curves (Fig. 12). Only the parameter $\Delta\bar{\theta}$ defined by (79) tends, on the average, to grow proportionally to $\bar{Q}^{1/3}$ with some similarity to (70):

$$\Delta\bar{\theta} = 3\bar{Q}^{1/3}. \tag{81}$$

In addition to $\Delta\bar{\theta}$, we illustrate in Fig. 15 one more parameter which characterizes the gain curve [see Fig.

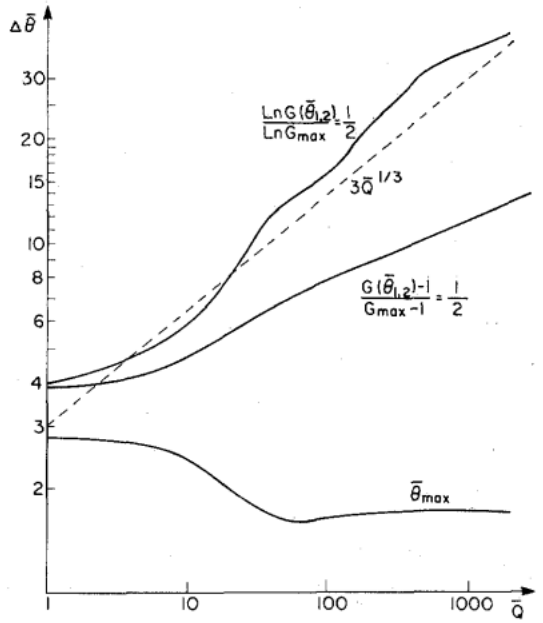


Fig. 15. The detuning bandwidth parameter $\Delta\bar{\theta}$, according to definitions (78) and (79), versus the gain parameter $\bar{Q}$. Only the curve corresponding to (79) tends on the average to a proportional dependence on $\bar{Q}^{1/3}$ (broken line). The lower curve displays the detuning parameter $\bar{\theta}_{max}$ for which maximum gain is obtained [see Fig. 17(a)].

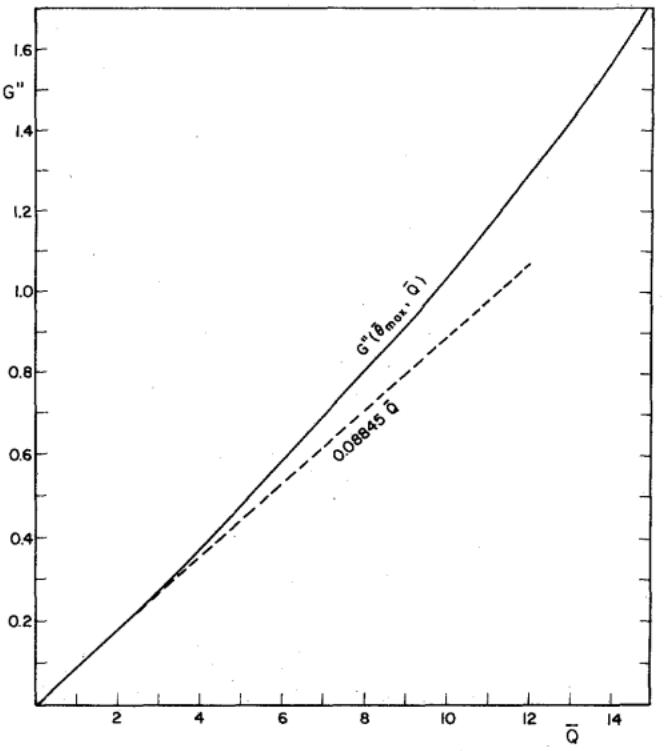


Fig. 16. The second derivative of the gain detuning function at the maximum gain point $G''(\bar{\theta}_{max}, \bar{Q})$ for a cold tenuous beam FEL. This parameter is used in (82) to calculate the $N$-transversal FEL gain bandwidth.

17(a)]—the maximum gain detuning point $\bar{\theta}_{max}$. This parameter is drawn for the parameters' regime $\theta_p \to 0$, $\bar{\theta}_{th} \to 0$. We note that in the low gain regime $\bar{\theta}_{max} \cong -2.6$ (as is well known). In the high gain regime $\bar{\theta}_{max}$ does not vanish, which explains the failure of the analytic approximation $G = \frac{1}{9}\exp(\sqrt{3}\,\bar{Q}^{1/3})$ (which was derived for $\bar{\theta} \simeq 0$) to be close to the exactly calculated gain, as mentioned before (Fig. 8).

When a FEL oscillator is being considered, a significant modification should be introduced to the estimate of $\Delta\bar{\theta}$. Considering an oscillator (or a regenerative amplifier), which builds up its power from a short injected pulse of seed radiation, the effective gain after $N$ round trips in the cavity is $[G_{net}(\bar{\theta})]^N$. For large $N$, this is, of course, a much narrower curve than $G(\bar{\theta})$, and it tends to a Lorentzian shape of width

$$\Delta\bar{\theta}_N = \sqrt{-\frac{2\ln 2}{N} \cdot \frac{G(\bar{\theta}_{max})}{G''(\bar{\theta}_{max})}} \tag{82}$$

as was shown in [40]. When the injected radiation is continuous (or when the oscillation buildup input power results from spontaneous emission), the stored power in the cavity accumulates from added contributions of new and recycled power in each round trip, and consequently grows as a geometrical series of single-path gain functions. Also, the $N$ round-trip gain function, which results from the summation of the series, has a detuning function width similar to (82).

The parameter $\Delta\bar{\theta}_N$ is useful for estimating the effective input power, which builds up the oscillation. This is a quantity which is needed for estimating the oscillation buildup time in finite macropulse accelerators [40]. We illustrate in Fig. 16 the computed values of $G''(\bar{\theta}_{max})$ as a function of $\bar{Q}$ for the limits $\bar{\theta}_p \to 0$, $\bar{\theta}_{th} \to 0$. The parameters read from Fig. 8, together with Fig. 16, can be used in (82) to calculate $\Delta\bar{\theta}_N$ in the high, low, or intermediate gain regimes.

In the low-gain limit $\bar{Q} \ll \pi$, the curve of $G''(\bar{\theta}_{max})$ tends to an asymptotic value $G''(\bar{\theta}_{max}) = 0.08845\,\bar{Q}$ (which can be calculated analytically from the low-gain regime detuning function). Substituted in (82), this results in an analytic expression for the $N$ transversals gain frequency bandwidth in the low-gain regime:

$$\frac{\Delta\omega_N}{\omega} = \frac{0.654}{N_w}\left[\frac{1 + (0.27\bar{Q})^{-1}}{N}\right]^{1/2}. \tag{83}$$

### *B. The Gain–Frequency Curve of a Waveguide FEL*

In the conclusion of this section, we consider briefly the question of the gain curve and gain bandwidth in a dispersive electromagnetic structure, and specifically, in a waveguide. Since in the formulation of our model we assumed an arbitrary value for the radiation mode wavenumber $k_z(\omega)$, the definition of the four operating parameters (35a)–(35d), and all the derived expressions and curves apply to any kind of dispersive electromagnetic mode (as long as the mode cross-section profile is uniform along the interaction length). The formulation specifically applies to waveguide modes, where the mode wavenumber is given by (73).

The only aspect in which the final results are different, in a dispersive electromagnetic structure, is in the gain curve dependence on frequency and the associated fre-

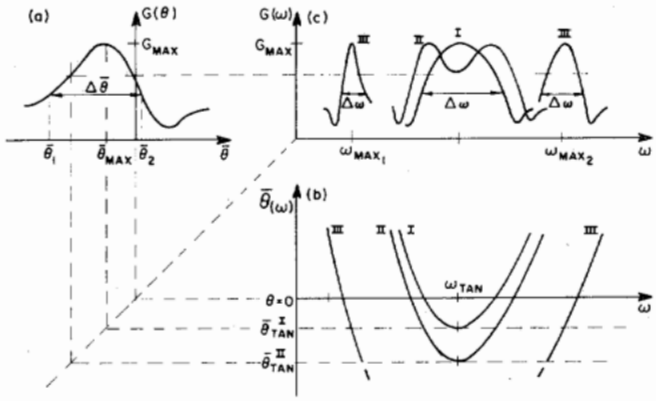


Fig. 17. Construction of the gain curve dependence on frequency $G(\omega)$ (c) out of the given gain detuning curve $G(\bar{\theta})$ (a) for a detuning parameter dependence on frequency $\bar{\theta}(\omega)$ corresponding to a waveguide dispersion relation (73) (b).

quency bandwidth parameters. However, if the dispersion relation $k_z(\omega)$ is known [in a waveguide, given by (73)], then the dependence of the detuning parameter $\bar{\theta}$ [see (23), (35d)] on $\omega$ is explicit and the gain curve dependence on frequency $G(\omega)$ can be drawn. Fig. 17 demonstrates the construction of $G(\omega)$ when $G(\theta)$ is known, and $\bar{\theta}(\omega) = [\omega/v_{z0} - (\omega^2 - \omega_{c0}^2)^{1/2}/c - k_w]L$ is the detuning parameter in a waveguide structure.

The function $\bar{\theta}(\omega)$ is clearly a function with a minimum. It attains its minimal value

$$\bar{\theta}_{\tan} = \left(\frac{\omega_{c0}}{\beta_{z0}\gamma_{z0}c} - k_w\right) L \tag{84}$$

at frequency

$$\omega_{\tan} = \gamma_{z0}\omega_{c0}. \tag{85}$$

At this frequency, the group velocity of the mode (the tangent to the dispersion curve) is equal to the beam velocity $v_{z0}$. If $\bar{\theta}_{\tan} \gg \bar{\theta}_2$ [$\bar{\theta}_2$ is the larger root of (78) or (79)], then at no frequency $\omega$ is gain available (in the low-gain regime, a sufficient condition for this is $\bar{\theta}_{\tan} > 0$). On the other hand, if $\bar{\theta}_{\tan} \ll \bar{\theta}_2$ (or $\bar{\theta}_{\max} - \bar{\theta}_{\tan} \ll \Delta\bar{\theta}/2$), then the construction of Fig. 17 results in two well-separated gain curves, which attain their maxima at

$$(\omega_{\max})_{1,2} = \gamma_{z0}^2\beta_{z0}c(k_w + \bar{\theta}_{\max}/L) \cdot \{1 \pm \sqrt{\beta_{z0}^2 - \omega_{c0}^2/[\gamma_{z0}(k_w + \bar{\theta}_{\max}/L)\, c]^2}\}. \tag{86}$$

In this limit, the linear approximation $\bar{\theta}(\omega) \simeq (\partial\bar{\theta}/\partial\omega)(\omega - \omega_0) = (v_{z0}^{-1} - v_{g0}^{-1})\, L(\omega - \omega_0)$ holds, and the two gain curves $G(\omega)$ are similar to the detuning curves $G(\bar{\theta})$ computed in this paper. The frequency bandwidth is given then by (74). Note that in the higher frequency gain curve $v_{g0} > v_{z0}$, and the opposite takes place in the lower frequency gain curve. Consequently, the two curves describing the gain dependence on frequency will look like mirror images of each other, but scaled in the frequency dimension by a different factor $|v_{z0}^{-1} - v_{g0_{1,2}}^{-1}|$ (see Fig. 17(c), curve III). The height of the two gain curves will be the same. Only when the two peak frequencies are different enough to change the constitutive parameters $\bar{Q}$, $\bar{\theta}_{\text{th}}$, will the maximum gains and the entire gain functions be different for both curves. This kind of two gain lines behavior was observed before, experimentally [44] and theoretically [45].

Note that, in order for the above discussion to apply, the waveguide FEL parameters must satisfy the inequalities

$$\beta_{z0} < \frac{\omega_{c0}}{k_w c} < \gamma_{z0}\beta_{z0}. \tag{87}$$

The right-hand side of the equality makes sure that (86) has a real solution (here we simplified the condition with the assumption $k_w L \gg \bar{\theta}_{\max}$, which makes (87) a condition for possible synchronization between the beam waves and the radiation mode). The left-hand side of the inequality (87) assures that $k_z(\omega_{\max_1}) > 0$, which corresponds to a forward propagating mode. In the opposite case,

$$\beta_{z0} > \frac{\omega_{c0}}{k_w c}, \tag{88}$$

the lower frequency solution is a backward propagating wave $k_{z_1} < 0$. This particular case may result in backward wave oscillations (absolute instability) in the FEL, and is not treated in the present article [46], [47].

In the intermediate regime $\bar{\theta}_1 \lesssim \bar{\theta}_{\tan} \lesssim \bar{\theta}_2$, the gain curve $G(\omega)$ may be quite dissimilar to $G(\bar{\theta})$ (see Fig. 17, curves I, II). Curve II demonstrates a double peak behavior of $G(\omega)$ [45] when $\bar{\theta}_{\tan} < \bar{\theta}_{\max}$. The frequency bandwidth may be made somewhat larger than (74), (75) (up to about a factor of 2), when this is a desirable feature. However, note that the maximum gain is not increased in this regime, and it is still bounded by $G_{\max} = G(\bar{\theta}_{\max})$. More accurate determination of the frequency bandwidth in this regime requires numerical computation.

For a complete quantitative description of the waveguide FEL gain curve, one should use also expressions for the gain parameter $\bar{Q}$ and space charge parameter $\bar{\theta}_p$, which are valid in a waveguide structure. The gain parameter $\bar{Q}$ of a waveguide FEL can be computed from the coupling coefficient expression (A6) and (31) and (35a). However, we note that the plasma frequency parameter $\omega_p'$, which is necessary for calculating $\omega_{c0}$ and $\bar{\theta}_p$, is also modified in a waveguide structure. There are different plasma frequency modification factors for the solenoidal and space charge waves of the system [45], [48]. Both modifications are ignored in the present work, which keeps the present waveguide FEL model valid only for $e$-beam transverse dimensions which are large, relative to the longitudinal wave wavelength $(k_{z0} + k_w)^{-1}$. Certainly, the formulation is valid in the tenuous beam regimes where space charge effects are totally negligible.

## VI. Conclusion

In this paper, we presented the general gain-dispersion relation of the FEL in terms of only four characteristic parameters: $\bar{Q}$, $\bar{\theta}_p$, $\bar{\theta}_{\text{th}}$, and $\bar{\theta}$. We defined the various gain

regimes, their analytic gain expressions, and their validity conditions in terms of these parameters. The analytic expressions were compared to the numerically calculated results and the relative errors were mapped for the various cases. The transitions between the gain regimes, where the relative error is high, were described with the aid of numerically calculated contour maps.

We introduced a number of alternative definitions for detuning spread acceptance, and showed their usefulness for estimating electron beam quality acceptance parameters and for evaluating the gain analytically in the intermediate regime. We also defined and calculated parameters of detuning bandwidth in amplifiers, oscillators, and waveguide FEL's. These parameters are useful, for example, for estimating the frequency bandwidth of the FEL and its beam energy instability acceptance.

In order to keep the analysis comprehensive and applicable for various devices and problems, we provided expressions for the coupling parameter $\kappa$ of various FEL kinds, and for the detuning spread parameters $\bar{\theta}_{\text{th}}$ corresponding to various causes for axial velocity spread of the electron beam.

In order to use the design tools provided by this paper, in a specific problem, the constitutive parameters $\bar{Q}$, $\bar{\theta}_p$, $\bar{\theta}_{\text{th}}$ must first be calculated. $\bar{\theta}_{\text{th}}$ can be calculated using the formulas of Appendix B. $\bar{\theta}_p$ is given by (27) and (35c), and $\bar{Q}$ is given by (31), (35a), and Appendix A. The second design stage is to find out if the FEL parameters fall well inside one of the analytic approximation gain regimes. If this is the case, the appropriate analytic expression for the gain and the maximum gain point may be used (Table I). The relative error can be estimated by Fig. 9 or 10(a) or (b). If the parameters lead to the intermediate or warm beam regimes and $\bar{\theta}_{\text{th}} \gg \bar{\theta}_p$, one may use the contours of Fig. 11 to estimate the gain. In a wide range of warm beam intermediate regime parameters, the gain can be estimated by the heuristic formula (71) and the curves of $\bar{\theta}_{th}^{ac}$ which are displayed in Fig. 14.

This procedure covers the entire parameters' range and provides a tool for the estimation of the FEL gain, without the need for complicated calculations.

## Appendix A
## The Coupling Parameter $\kappa$

The coupling parameter $\kappa$ measures the strength of the coupling between the electromagnetic wave and the electron beam plasma waves. While the other parameters of the model depend only on the properties of the electron beam, $\kappa$ is the only parameter which is dependent on the specific scheme of FEL considered. This way, the gain-dispersion relation (4) is a generic formula for various kinds of FEL's.

Expressions for $\kappa$ for various FEL's are given and discussed in [9] and listed again for convenience in Table III.

$A_e$ is the electron beam cross-section area and $\mathcal{E}_{z0}(x, y)$ is the longitudinal electric field profile function of the electromagnetic mode.

$\mathcal{E}_{z1}(x, y)$ is the longitudinal electric field profile function

TABLE III
The Coupling Parameter $\kappa$ of Various FEL's (The Highly Relativistic Limit Expressions Are Given in Brackets)

| FEL | $\kappa$ |
|---|---|
| Cerenkov | $\frac{\pi\sqrt{\epsilon/\mu}}{2\lambda\mathcal{P}}\iint_{A_e}\lvert\mathcal{E}_{z0}(x, y)\rvert^2\,dx\,dy$ |
| Smith–Purcell | $\frac{\pi\sqrt{\epsilon/\mu}}{2\lambda\mathcal{P}}\iint_{A_e}\lvert\mathcal{E}_{z1}(x, y)\rvert^2\,dx\,dy$ |
| Longitudinal electrostatic | $\alpha^2\frac{\pi\sqrt{\epsilon/\mu}}{2\lambda\mathcal{P}}\iint_{A_e}\lvert\mathcal{E}_{z0}(x, y)\rvert^2\,dx\,dy$ |
| Transverse electrostatic | $\frac{1}{8\pi}\left(\frac{e\bar{E}_w}{mc^2}\right)^2\frac{(1+\beta_{0z})^2}{\beta_{0z}}\frac{\gamma_{0z}^4}{\gamma_0^2}\frac{A_e}{A_{\text{EM}}}\lambda$ $\left[\frac{\lambda}{2\pi}\left(\frac{e\bar{E}_w}{mc^2}\right)^2\frac{\gamma_{0z}^4}{\gamma_0^2}\frac{A_e}{A_{\text{EM}}}\right]$ |
| Magnetic brehmsstrahlung | $\frac{1}{8\pi}\left(\frac{e\bar{B}_wc}{mc^2}\right)^2(1+\beta_{0z})^2\frac{\gamma_{0z}^4}{\gamma_0^2}\frac{A_e}{A_{\text{EM}}}\lambda$ $\left[\frac{\lambda}{2\pi}\left(\frac{e\bar{B}_wc}{mc^2}\right)^2\frac{\gamma_{0z}^4}{\gamma_0^2}\frac{A_e}{A_{\text{EM}}}\right]$ |
| Compton–Raman | $\frac{1}{2\pi}\left(\frac{e\bar{E}_w}{mc^2}\right)^2(1+\beta_{0z})^2\frac{\gamma_{0z}^4}{\gamma_0^2}\frac{A_e}{A_{\text{EM}}}\lambda$ $\left[\frac{\lambda}{\pi}\left(\frac{e}{mc^2}\right)^2\left(\frac{\mu_0}{\epsilon_0}\right)^{1/2}S_w\frac{\gamma_{0z}^4}{\gamma_0^2}\frac{A_e}{A_{\text{EM}}}\right]$ |

of the first-order space harmonic of the electromagnetic mode in the Smith–Purcell periodic waveguide, given by

$$\mathcal{E}_{z1}(x, y) = \frac{1}{\lambda_w}\int_0^{\lambda_w} e^{-i(k_{z0}+k_w)z}\,E_z(x, y, z)\,dz \quad \text{(A1)}$$

where $\lambda_w$ is the period of the periodic electromagnetic structure. $\mathcal{P}$ is the total electromagnetic power of the uncoupled mode:

$$\mathcal{P} = \tfrac{1}{2}\int_{-\infty}^{\infty}\int \text{Re}[\mathcal{E}(x, y, z) \times \mathcal{H}^*(x, y, z)] \cdot \hat{t}_z\,dx\,dy. \quad \text{(A2)}$$

For a longitudinal electrostatic FEL [15], the parameter $\alpha^2$ is defined by

$$\alpha^2 = \left(\frac{1}{2\beta_0^2\gamma_0^3}\cdot\frac{L}{\lambda}\cdot\frac{e\phi_w}{mc^2}\right)^2 \quad \text{(A3)}$$

where $\phi_w = E_w/k_w$ is the amplitude of the periodic electrostatic potential in this laser. In this case, $\chi(\omega, s)$ must be replaced in the gain-dispersion relation (4) by

$$\chi(\omega, s) = (1 + \alpha^2)\,\chi_p(\omega, s) \quad \text{(A4)}$$

where $\chi_p$ is given by (6).

In all longitudinal interaction FEL's (rows 1–3), the magnetized plasma approximation was used in deriving the expressions for $k$.

For transverse electrostatic FEL [15], [16], $\bar{E}_w$ is the rms electrostatic field of the transverse wiggler, and for magnetic bremsstrahlung FEL [10], [11], $\bar{B}_w$ is the rms magnetic wiggler field (either linear or helical). In the

Compton–Raman FEL [8], the electron beam is pumped by a time-varying electromagnetic wave, propagating in counterdirection to the electron beam with a Poynting vector power density $S_w$ and transverse electric field amplitude $E_w$. In all the transverse FEL schemes (rows 4–6), the coupling coefficient is calculated specifically for a TEM radiation mode. The parameter $A_{\mathrm{EM}}$ in these cases is the effective electromagnetic mode area defined by

$$A_{\mathrm{EM}} = \mathcal{P}\left[\tfrac{1}{2}\sqrt{\epsilon/\mu}\,|\mathcal{E}(x_e, y_e)|^2\right] \tag{A5}$$

where $x_e$, $y_e$ are the electron beam coordinates.

The FEL scheme of most interest is the magnetic bremsstrahlung FEL. For this device, we calculated the coupling coefficient separately in a model which includes also waveguide effects [47]. The result can be written in the highly relativistic limit in the compact way:

$$\kappa = \frac{1}{4}\frac{A_e}{A_{\mathrm{EM}}}\left(\frac{\bar{a}_w}{\gamma_0}\right)^2 k_{z0} \tag{A6}$$

where $\bar{a}_w = e\bar{B}_w/(k_w mc)$.

In the limit of nondispersive electromagnetic structure ($k_z = \omega/c$, $\lambda = \lambda_w/2\gamma_{z0}^2$), (A6) reduces to the expression in row 5 of Table III. For the purpose of convenience in application, we also list here explicitly the conventional expression for the gain parameter $\bar{Q}$ corresponding to this specific case:

$$\bar{Q} = 8\sqrt{2}\,\pi^2 \frac{r_e}{c}\frac{I_0}{e}\frac{\lambda^{3/2}L^3}{A_{\mathrm{EM}}\lambda_w^{3/2}}\frac{\bar{a}_w^2}{(1+\bar{a}_w^2)^{3/2}} \tag{A7}$$

where

$$r_e = e^2/(4\pi\epsilon_0 mc^2) = 2.818 \times 10^{-15}\ \mathrm{m}$$

is the classical electron radius and $I_0$ is the instantaneous beam current.

We note that in the case of a strong linear wiggler (high harmonics operating regime) $\bar{a}_\omega >> 1$, the coupling and gain parameters (A6) and (A7) should be modified by a reduction factor of

$$[JJ] = \left[J_0\left(\frac{\bar{a}_w^2/2}{1+\bar{a}_w^2}\right) - J_1\left[\frac{\bar{a}_w^2/2}{1+\bar{a}_w^2}\right)\right]^2 \tag{A8}$$

where $J_0$, $J_1$ are the zero- and first-order Bessel functions, respectively [49]. With this modification, the gain dispersion (4) continues to be valid, at least in the tenuous beam regimes. The effects of space charge and operation at high harmonics are described in [49].

## Appendix B
## The Detuning Spread Parameter $\bar{\theta}_{\mathrm{th}}$

The axial velocity spread of the electron beam generally causes a reduction in the gain of the FEL. The various sources for the axial velocity spread are discussed in [40] and briefly summarized in Table IV, for the highly relativistic limit $\beta_z \to 1$. Note, however, that the free space propagation assumption ($k_{z0} = \omega/c$) is not used, and the expressions for $\bar{\theta}_{\mathrm{th}}$ apply also for dispersive electromagnetic structures like a waveguide (73).

TABLE IV
Axial Velocity and Detuning Spread Parameter

| Spread source | $v_{z\mathrm{th}}/c$ | $\bar{\theta}_{\mathrm{th}}$ |
|---|---|---|
| Energy spread | $\frac{1}{2\gamma_z^2}\frac{\Delta E}{E}$ | $\frac{\pi}{\gamma_z^2}\frac{\Delta E}{E}\frac{L}{\lambda}$ |
| Angular spread | $\frac{(\epsilon/\pi)^2}{2 r_{b0}^2}$ | $\frac{1}{\pi}\frac{\epsilon^2}{r_{b0}^2}\frac{L}{\lambda}$ |
| Transverse gradient | $\frac{1}{2}k_\beta^2 r_b^2$ | $\pi k_\beta^2 r_b^2 L/\lambda$ |
| Emittance (minimal) | $\frac{1}{2\pi}k_\beta\epsilon$ | $k_\beta\epsilon L/\lambda$ |
| Space charge | $3\times10^{-5}\times\frac{1}{\gamma_z^2\gamma}I_0$ | $6\pi\times10^{-5}\times\frac{I_0}{\gamma_z^2\gamma}\frac{L}{\lambda}$ |

The total energy spread parameter $\Delta E$ (row 1) is the FWHM energy spread $\Delta E = \Delta\gamma mc^2$. For a Gaussian energy distribution, $\Delta E$ is defined as $\Delta E \simeq 2E_{\mathrm{th}}$ where $E_0 \pm E_{\mathrm{th}}$ are the $1/e$ falloff points of the energy distribution. When an RF linac is used, $\Delta E$ is attributed mostly to the finite phase bunching of the electron microbunches in the acceleration gaps.

The emittance $\epsilon$ (row 2) is defined by

$$\epsilon = \pi r_{b0}\Theta_b \tag{B1}$$

where $r_{b0}$ is the initial beam radius and $\Theta_b$ is the half opening angle of the angular spread. The emittance is a beam parameter which is independent of the focusing apparatus. It is limited in most RF accelerators by the phenomenological "Lawson–Penner" relation [43], although many well-designed accelerators have a lower emittance than that given by this limit. In particular, much smaller emittance values are available in storage ring beams. The finite emittance corresponds to a finite transverse velocity spread of the electrons in the wiggler, and consequently (if the total velocity spread is negligible) results in the axial velocity spread given in row 2.

Another source for the transverse spread is the transverse gradient in the wiggler field (row 3), which is present in any realizable wiggler. This transverse gradient produces a gradient in the electrons' transverse quiver velocity (corresponding to their transverse position), and consequently causes a spread in the axial velocity of a finite width monoenergetic beam, which propagates along the wiggler axis. The transverse gradient also produces a focusing effect on the beam which causes the electrons to perform long wavelength (betatron) oscillations with an oscillation wavenumber [40]:

$$k_\beta = \frac{a_w}{\sqrt{2}\beta_z\gamma}k_w \tag{B2}$$

where $a_w = eB_w/k_w mc$ is the normalized vector potential of the wiggler magnetic field amplitude $B_w$. $r_b$ is the maximum radius of the beam envelope inside the wiggler.

For a long enough wiggler, minimal axial velocity spread is attained when the electron beam is inserted with an optimal beam radius:

$$r_{b0} = \left(\frac{\epsilon}{\pi k_\beta}\right)^2. \tag{B3}$$

In this condition, as noted in [40], the beam envelope is uniform and the total emittance contribution due to both the transverse gradient and the angular spread is minimal and listed in line 4.

The potential depression across a dense, nonneutralized electron beam also contributes axial velocity spread (row 5). $I_0$ is the beam peak current, expressed in amperes.

In calculating the total detuning spread parameter $\bar{\theta}_{\text{th}}$, one should add in quadratures the contributions of the angular spread and the transverse gradient to $\bar{\theta}_{\text{th}}$. Other contributions add up in a more complicated way and usually generate a total axial velocity distribution which is not necessarily Gaussian [50]. A "worst case" estimate for the total detuning parameter spread would be obtained by adding the contributions linearly. When the exact distribution function is known, $v_{z\text{th}}/c$ and consequently $\bar{\theta}_{\text{th}} = (v_{z\text{th}}/c)\ (2\pi L/\lambda)$ can be calculated by fitting a Gaussian to the given distribution.

Table IV applies for both linear and helical wiggler cases. Note, however, that in a linear wiggler, there is a transverse gradient focusing effect and betatron oscillation only in the polarization plane (perpendicularly to the wiggling plane).

## References


[1] L. R. Elias, W. Fairbank, J. Madey, H. A. Schwettman, and T. Smith, "Observation of stimulated emission of radiation by relativistic electrons in a spatially periodic transverse magnetic field," *Phys. Rev. Lett.*, vol. 36, pp. 717–720, 1976.

[2] D. A. G. Deacon, L. R. Elias, J. M. J. Madey, G. J. Ramian, H. A. Schwettman, and T. I. Smith, "First operation of free electron laser," *Phys. Rev. Lett.*, vol. 38, pp. 892–894, 1977.

[3] D. B. McDermott, T. C. Marshall, S. P. Schlesinger, R. K. Parker, and V. L. Granatstein, "High power free electron laser based on stimulated Raman backscattering," *Phys. Rev. Lett.*, vol. 41, pp. 1368–1371, 1978.

[4] J. E. Walsh, T. C. Marshall, and S. P. Schlesinger, "Generation of coherent Cerenkov radiation with an intense relativistic electron beam," *Phys. Fluids*, vol. 20, pp. 709–710, 1977.

[5] J. A. Edighoffer, W. D. Kimora, R. H. Pantell, M. A. Piestrup, and D. Y. Wang, "Observation of inverse Cerenkov interaction between free electrons and laser light," *Phys. Rev. A*, vol. 23, pp. 1848–1854, 1981.

[6] R. M. Phillips, "The Ubitron—A high power millimeter wave TWT," *IRE Trans. Electron Devices*, vol. ED-7, p. 231, 1960.

[7] K. Mizuno, S. Ono, and Y. Shibata, "Two different mode interactions in an electron tube with a Fabry Perot resonator—The Ledatron," *IEEE Trans. Electron Devices*, vol. ED-20, pp. 749–752, 1973.

[8] P. Sprangle and A. T. Drobot, "Stimulated backscattering from relativistic unmagnetized electron beams," *J. Appl. Phys.*, vol. 50, pp. 2652–2661, 1979.

[9] A. Gover and P. Sprangle, "A unified theory of magnetic bremsstrahlung, electrostatic bremsstrahlung, Compton–Raman scattering, and Cerenkov–Smith–Purcell free electron lasers," *IEEE J. Quantum Electron.*, vol. QE-17, pp. 1196–1215, 1981.

[10] N. M. Kroll and W. A. McMullin, "Stimulated emission from relativistic electrons passing through a spatially periodic transverse magnetic field," *Phys. Rev.*, vol. A17, pp. 300–308, 1978.

[11] P. Sprangle and R. Smith, "Theory of free electron lasers," *Phys. Rev.*, vol. A21, pp. 293–301, 1980.

[12] L. B. Bernstein and J. L. Hirshfield, "Amplification on a relativistic electron beam in a spatially periodic transverse magnetic field," *Phys. Rev.*, vol. A20, pp. 1661–1670, 1979.

[13] F. A. Hopf, P. Meystre, M. O. Scully, and W. H. Louisell, "Classical theory of free electron laser," *Phys. Rev. Lett.*, vol. 37, pp. 1342–1345, 1976.

[14] W. B. Colson, "One body analysis of free electron lasers," in *Physics of Quantum Electronics*, vol. 5, S. Jacobs, M. Sargent III, and M. O. Scully, Eds. Reading, MA: Addison-Wesley, 1978, pp. 157–196.

[15] A. Gover, "A free electron laser based on periodic longitudinal electrostatic bremsstrahlung," in *Physics of Quantum Electronics*, vol. 7, S. Jacobs, H. Pilloff, M. Sargent III, and M. O. Scully, Eds. Reading, MA: Addison-Wesley, 1980, pp. 701–728.

[16] G. Bekefi and R. E. Shefer, "Stimulated Raman scattering by an intense relativistic electron beam subjected to a rippled electric field," *J. Appl. Phys.*, vol. 50, pp. 5158–5164, 1979.

[17] A. Gover and A. Yariv, "Collective and single electron interaction of electron beams with electromagnetic waves, and free electron lasers," *Appl. Phys.*, vol. 16, pp. 121–138, 1978.

[18] A. Gover and Z. Livni, "Operation regime of Cerenkov–Smith–Purcell free electron lasers and T. W. amplifiers," *Opt. Commun.*, vol. 26, pp. 375–380, 1978.

[19] J. E. Walsh, "Stimulated Cerenkov radiation," in *Physics of Quantum Electronics*, vol. 5, J. Jacobs, M. Sargent III, and M. O. Scully, Eds. Reading, MA: Addison-Wesley, 1978, pp. 357–380.

[20] C. C. Shih and A. Yariv, "Inclusion of space charge effects with Maxwell's equations in the single particle analysis of free electron lasers," *IEEE J. Quantum Electron.*, vol. QE-17, pp. 1387–1394, 1981.

[21] M. A. Piestrup and P. F. Finman, "The prospect of an X-ray free electron laser using stimulated resonance transition radiation," *IEEE J. Quantum Electron.*, vol. QE-19, pp. 357–364, 1983.

[22] J. R. Pierce, *Travelling Wave Tubes*. Princeton, NJ: Van Nostrand, 1950.

[23] T. M. O'Neil and J. H. Malberg, "Transition of the dispersion roots from beam-type to Landau-type solutions," *Phys. Fluids*, vol. 11, pp. 1754–1760, 1968.

[24] M. A. Piestrup, "Multiple beam free electron lasers and optical klystrons," *Appl. Phys. Lett.*, vol. 39, pp. 696–698, 1981.

[25] S. Cuperman, F. Petran, and A. Gover, "Electromagnetic instability supported by a rippled, magnetically focused relativistic electron beam," *J. Plasma Phys.*, vol. 31, part 2, pp. 329–351, 1984.

[26] Z. Livni and A. Gover, "Linear analysis and implementation considerations of free electron lasers based on Cerenkov and Smith–Purcell effects," Quantum Electron. Lab., Sch. Eng., Tel-Aviv Univ., Tel-Aviv, Israel, Sci. Rep. 1979/1 (AFOSR 77-3445), 1979.

[27] M. Abramowitz and I. A. Stegun, Eds., *Handbook of Mathematical Functions*. New York: Dover, 1972.

[28] B. D. Fried and S. D. Conte, *The Plasma Dispersion Function*. New York: Academic, 1961.

[29] K. H. Burell, "An investigation of the resonance cone structure in warm unisotropic plasma," Ph.D. dissertation, California Inst. Technol., Pasadena, 1974.

[30] H. E. Salzer, "Additional formulas and tables for orthogonal polynomials originating from inversion integrals," *J. Math. Phys.*, vol. 40, p. 72, 1961.

[31] ——, "Orthogonal polynomials arising in the numerical evaluation of inverse Laplace transform," *Math. Tables Other Aids Comput.*, vol. 9, p. 164, 1955.

[32] A. Stroud and D. Secrest, *Gaussian Quadrature Formulas*. Englewoods Cliffs, NJ: Prentice-Hall, 1966.

[33] T. C. Marshall, S. P. Schlesinger, and D. B. McDermott, "The free electron laser: A high-power submillimeter radiation soruce," in *Advances in Electronics and Electron Physics*, vol. 53, C. Marton, Ed. New York: Academic, 1980, pp. 47–84.

[34] A. Hasegawa, "Free electron laser," *Bell Syst. Tech. J.*, vol. 57, pp. 3069–3089, 1978.

[35] G. Dattoli, A. Marino, A. Renieri, and F. Romanelli, "Progress in the Hamiltonian picture of the free electron laser," *IEEE J. Quantum Electron.*, vol. QE-17, pp. 1371–1387, 1981.

[36] L. F. Ibanez and S. Johnston, "Finite temperature effects in free electron lasers," *IEEE J. Quantum Electron.*, vol. QE-19, pp. 339–346, 1983.

[37] A. Fruchtman and J. L. Hirshfield, "Degradation in gain for free electron laser amplifier due to electron momentum spread," *Int. J. Infrared Millimeter Waves*, vol. 2, pp. 905–913, 1981.

[38] I. Boscolo, M. Leo, R. A. Leo, G. Soliani, and V. Stagno, "On the

gain of the free electron laser (FEL) amplifier for a nonmonoenergetic beam," *IEEE J. Quantum Electron.*, vol. QE-18, pp. 1957–1961, 1982.
[39] D. B. McDermott, "Effect of velocity spread on finite length free electron laser gain," *Int. J. Infrared Millimeter Waves*, vol. 4, p. 1015–1027, 1983.
[40] A. Gover, H. Freund, V. L. Granatstein, J. H. McAdoo, and C.-M. Tang, "Basic design considerations for FELs driven by electron beams from RF accelerators," NRL Rep. 8747; also in *Infrared and Millimeter Waves*, vol. 11, ch. 8,, K. J. Button, Ed. New York: Academic, 1984.
[41] A. Gover and E. Jerby, "The axial velocity spread acceptance of free electron lasers," Quantum Electron. Lab., Tel-Aviv University, Faculty Eng., Tel-Aviv, Israel, Sci. Rep. QE-3/84; also in *Free Electron Laser Conf. Proc.*, Castel Gandolfo, Rome, Italy, 1984, to be published in *Nucl. Instrum. and Methods in Phys. Res. A*, 1985.
[42] R. C. Davidson and H. S. Uhm, "Self consistent Vlasov description of the free electron laser instability," *Phys. Fluids*, vol. 23, pp. 2076–2084, 1980.
[43] V. K. Neil, "Emittance and transport of electron beams in a free electron laser," JASON Tech. Rep. JSR-79-10, 1979.
[44] J. Fajans, G. Bekefi, Y. Z. Yin, and B. Lax, "Spectral mesurements from a tunable, Raman, free electron laser," *Phys. Rev. Lett.*, vol. 53, pp. 246–249, 1984.
[45] H. P. Freund and A. K. Ganguly, "Three-dimensional theory of the free electron laser in a collective regime," *Phys. Rev. A*, vol. 28, pp. 3438–3448, 1983.
[46] P. C. Liewer, A. T. Lin, and J. M. Dawson, "Theory of an absolute instability of a finite length free electron laser," *Phys. Rev. A*, vol. 23, pp. 1251–1255, 1981.
[47] B. Steinberg, A. Gover, and S. Ruschin, "A unified analysis of absolute and convective instabilities in stimulated Compton-Raman scattering and free electron lasers."
[48] G. M. Branch and T. G. Mihran, "Plasma frequency reduction factors in electron beams," *IRE Trans. Electron Devices*, vol. ED-2, pp. 3–11, 1955.
[49] E. Jerby and A. Gover, "A small signal gain analysis of a planar wiggler FEL, operating in the high harmonic (strong wiggler) regime," to be published.
[50] —, "An exact electron momentum distribution kinetic analysis of the free electron laser," to be published.

**E. Jerby** was born in Israel in 1957. He received the B.Sc. degree in electrical engineering and the M.Sc. degrees from Tel-Aviv University, Tel-Aviv, Israel, in 1980.

Since November 1983 he has been a Ph.D. student at Tel-Aviv University, where he is theoretically studying the gain-dispersion relations of free electron lasers.

**A. Gover** (S'72–M'75–SM'82) was born in Poland in 1945. He received the B.S. degree in physics and the M.S. degree in solid-state physics from Tel-Aviv University, Tel-Aviv, Israel, in 1968 and 1972, respectively, and the Ph.D. degree in applied physics from the California Institute of Technology, Pasadena, in 1975.

He has been employed by Tadiron Electronic Industries, Israel, the California Institute of Technology, and Stanford University, Stanford, CA. He has been Consultant to Spectrolab and Meret in California, and recently to Jaycor and S.A.I. in Washington, DC. Since 1977, he has been a member of the Faculty of Engineering of Tel-Aviv University, in the Department of Electron Devices and Materials and Electromagnetic Radiation. He is conducting research in the fields of quantum electronics, electron devices, and free electron lasers.

Dr. Gover is a member of the Optical Society of America.